nanomaterials

MDPI

Article

A Processing Window for MoS_2/WS_2 Heterostructures by Sulphurisation of Sputtered Precursors

Florinel Sava [1], Iosif-Daniel Simandan [1], Claudia Mihai [1], Mohamed Yassine Zaki [2], Dan Nicolae Becherescu Barbu [3] and Alin Velea [1,*]

[1] National Institute of Materials Physics, Atomistilor 405A, 077125 Magurele, Romania; fsava@infim.ro (F.S.); simandan@infim.ro (I.-D.S.); claudia.mihai@infim.ro (C.M.)
[2] Department of Materials Science, Energy and Nano-Engineering (MSN), College of Chemical Sciences and Engineering (CCSE), Mohammed VI Polytechnic University (UM6P), Benguerir 43150, Morocco; mohamedyassine.zaki-ext@um6p.ma
[3] Phanos Technology S.R.L., C. A. Rosetti 14, 235300 Corabia, Romania; nicu.becherescu@phanos.ro
* Correspondence: alin.velea@infim.ro

Abstract

MoS_2/WS_2 heterostructures can be grown over large areas by sulphurising sputtered precursors, but Mo-W interdiffusion across the interface limits the usable temperature. Metallic Mo/W and sulphide MoS_x/WS_x stacks, sputtered at room temperature or with one or both layers at 500 °C, were sulphurised in a confined graphite box for 15 min between 500 and 700 °C, and characterised by X-ray reflectivity and diffraction, Raman spectroscopy at 532 and 633 nm and electron microscopy. For room-temperature precursors, sulphurisation at 550 to 650 °C produced crystalline, textured MoS_2 and WS_2, with a separation of 9.3 to 10.3 cm^{-1} between the A_{1g} Raman bands at the sample centre. At 500 °C both disulphides formed from the metallic stack, while the sulphide WS_x layer did not crystallise. At 700 °C the two A_{1g} bands converged, the crystallite size doubled and the reflectivity fringes were damped, which we attribute to Mo-W mixing. Precursors deposited at 500 °C and sulphurised at 650 °C showed no larger A_{1g} separation, and the metallic stacks showed the same band convergence near the sample edges. Sulphurisation of room-temperature precursors at 550 to 650 °C thus produces MoS_2/WS_2 heterostructures with separate MoS_2 and WS_2 Raman bands in a single step.

Keywords: MoS_2/WS_2 heterostructures; sulphurisation; magnetron sputtering; interdiffusion; $Mo_{1-x}W_xS_2$; Raman spectroscopy; resonance Raman; X-ray reflectivity; transition metal dichalcogenides

Check for updates

Academic Editor: Werner Blau

Received: 30 October 2026
Revised: 15 November 2026
Accepted: 16 November 2026
Published: 18 November 2026

Copyright: © 2026 by the authors. Licensee MDPI, Basel, Switzerland. This article is an open access article distributed under the terms and conditions of the Creative Commons Attribution (CC BY) license.

1. Introduction

Molybdenum disulphide (MoS_2) and tungsten disulphide (WS_2) are layered semiconductors that can be stacked by van der Waals bonding into vertical heterostructures [1–3]. The MoS_2/WS_2 pair has a type II band alignment [4], so that holes transfer from MoS_2 to WS_2 within 50 fs after optical excitation [5] and interlayer excitons form across the interface [6]. These properties are the basis of the interest in MoS_2/WS_2 stacks for photodetectors and diodes, and they depend on an abrupt interface between the two disulphides. $Mo_{1-x}W_xS_2$ alloys are random solid solutions over the whole composition range [7], with an ordering temperature calculated at approximately 36 K [8]. A sharp MoS_2/WS_2 interface is therefore not an equilibrium state, and it persists only as long as Mo and W do not interdiffuse across it. When Mo and W interdiffuse, a graded $Mo_{1-x}W_xS_2$ layer forms, whose band gap and exciton energies vary with composition [9,10].

Devices made from such stacks require growth over large areas. Metal–organic chemical vapour deposition produces wafer-scale MoS_2 and WS_2 with high electronic quality [11]. A simpler route is the sulphurisation of thin precursor films deposited by magnetron sputtering, which is scalable and produces layer-controlled MoS_2 and WS_2 [12,13]. The precursor can be a metal or an amorphous sulphide sputtered from a MoS_2 or WS_2 target [14,15]. Amorphous MoS_2 sputtered directly on graphene and crystallised in a confined sulphurisation step has been used in lateral MoS_2/graphene memristors without polymer transfer [16]. Sulphurisation of thin Mo and W films for 15 min produces mostly stoichiometric disulphides at 550 °C [17], which is above the limit of 400 °C for back-end-of-line processing [18]. The temperature of the sulphurisation step therefore has to be chosen against two limits, complete sulphurisation of both precursor layers on one side and the onset of Mo-W interdiffusion on the other.

Reports on heterostructures made in this way differ on the temperature of the second limit. Mo sputtered on W and sulphurised at 600 °C for 2 h resulted in a nearly atomically sharp MoS_2/WS_2 interface without alloying, with diode rectification above 10^3 [19]. A sputtered W and Mo stack sulphurised at 750 °C for 15 min also showed the separate Raman modes of MoS_2 and WS_2 [20]. In contrast, a Mo film on a W film, each 1.2 nm thick, sulphurised at 700 °C resulted in a uniform $Mo_{0.5}W_{0.5}S_2$ film, attributed to the interdiffusion of Mo and W in the stack [21]. In our previous work, MoS_x sputtered on W and sulphurised in a confined graphite box at 800 to 850 °C resulted in vertically graded $Mo_{1-x}W_xS_2$ multilayers [22]. Two-step processes, in which the first disulphide is fully formed before the second metal is deposited and sulphurised, were developed to avoid this mixing [23]. A composition gradient is not always a defect, since a designed vertical $Mo_{1-x}W_xS_2$ profile can improve photodetection [10] and $Mo_{1-x}W_xS_2$ layers respond over the visible range in photoconductive devices [24], but such a gradient has to be controlled by the process.

The temperature range in which sulphurisation transforms a sputtered stack into two separate disulphides has not been determined for one process, and the effect of the precursor on this range has not been examined. The chemical state of the precursor affects its sulphurisation. Metallic Mo films a few nanometres thick oxidise in air before sulphurisation, while amorphous MoS_x and WS_x already contain metal-sulphur bonds [15,17]. Sulphurisation in the confined graphite box used in this work resulted in MoS_2 films of different textures from sulphide and metallic precursors [25], in WS_2 from sputtered films [26], and in WS_2 from a monolayer WO_x film at 450 °C [27]. The deposition temperature is a further variable, because the density and the stoichiometry of the precursor layers depend on the substrate temperature.

In this work, metallic Mo/W and sulphide MoS_x/WS_x stacks were deposited by magnetron sputtering at room temperature and with one or both layers at 500 °C, and sulphurised in a confined graphite box for 15 min at 500 to 700 °C. For the precursors deposited at room temperature, sulphurisation between 550 and 650 °C produced crystalline disulphides from both layers, with the MoS_2 and WS_2 Raman bands remaining separate at the sample centre, and the two A_{1g} bands moved toward each other at 700 °C. At 500 °C both disulphides already formed from the metallic precursor, while the WS_x layer of the sulphide precursor did not crystallise. Precursors with one or both layers deposited at 500 °C and sulphurised at 650 °C showed no larger separation of the two sets of bands. The Mo layer deposited at room temperature on W deposited at 500 °C was fully oxidised before sulphurisation, half of the MoS_x deposited at 500 °C remained on the substrate, and the metallic stacks deposited at 500 °C showed convergence of the A_{1g} bands near the sample edges at 650 °C. These results define a processing window for MoS_2/WS_2 heterostructures obtained by sulphurisation of sputtered precursors.

2. Materials and Methods

2.1. Deposition of the Precursor Stacks

Precursor stacks were deposited by radio-frequency (RF) magnetron sputtering on SiO_2 (90 nm)/Si substrates of 20 mm × 15 mm (MicroChemicals GmbH, Ulm, Germany), cleaned with acetone, isopropyl alcohol and deionised water. The targets were W, Mo, WS_2 and MoS_2 (Mateck GmbH, Jülich, Germany, 99.9% purity, 5 cm diameter, 3 mm thickness). The target-to-substrate distance was 12 cm, and the substrates were rotated during deposition to obtain a uniform thickness. The base pressure before admitting the gas was between 6.9×10^{-5} and 9.5×10^{-5} Torr. The sputtering system and the deposition of ultrathin MoS_x and W layers at low rates were described previously [22]. Deposition was carried out in Ar at a flow of 30 sccm, at a working pressure between 4.0×10^{-3} and 5.3×10^{-3} Torr. The power on each target was set by calibrating the deposition rate with a quartz crystal microbalance (Inficon, Bad Ragaz, Switzerland) at 6×10^{-3} Torr, and each target was pre-sputtered for 5 min before deposition. In every stack the W-based layer was deposited first and the Mo-based layer second.

Two precursor chemistries were used. Metallic stacks (Mo on W) were deposited from the W and Mo targets, and sulphide stacks (MoS_x on WS_x) from the WS_2 and MoS_2 targets. Each chemistry was deposited in three thermal configurations, with both layers at room temperature, with both layers at a substrate temperature of 500 °C, and with the W-based layer at 500 °C and the Mo-based layer at room temperature. For depositions at 500 °C the substrate heater was started approximately 150 min before deposition, and the substrate temperature measured during deposition was between 494 and 509 °C. In the configuration with only the W-based layer heated, the heater was switched off after the first layer and the Mo-based layer was deposited the following day at 23 °C, without opening the chamber. The six precursors are shown schematically in Figure 1a, and the deposition conditions are summarised in Table 1.

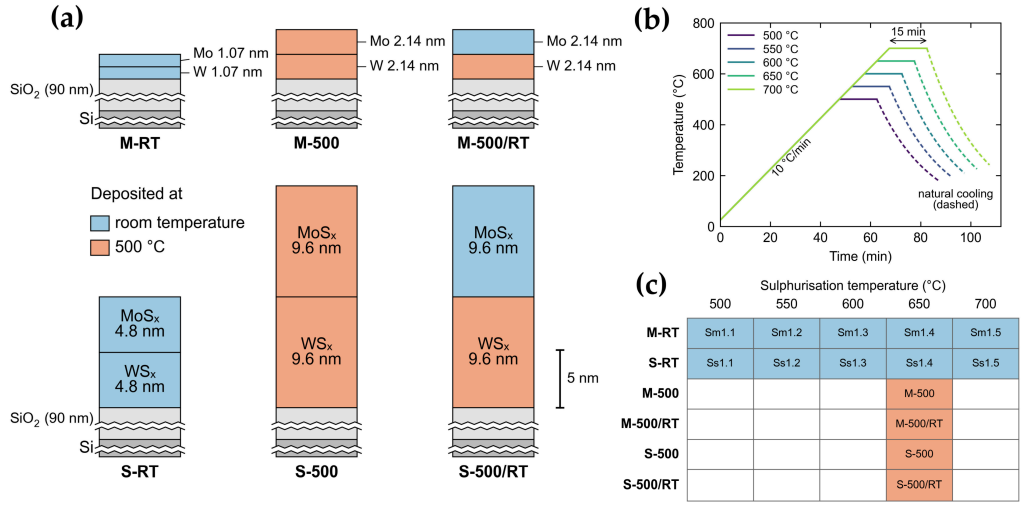


Figure 1. Precursor stacks and sulphurisation. (**a**) Schematic cross-sections of the six precursor stacks on SiO_2 (90 nm)/Si, metallic Mo on W (M-RT, M-500, M-500/RT) and sulphide MoS_x on WS_x (S-RT, S-500, S-500/RT), with the nominal layer thicknesses and the substrate temperature during the deposition of each layer. (**b**) Temperature profiles of the sulphurisation in the confined graphite box, heating at 10 °C/min to a hold of 15 min at 500, 550, 600, 650 or 700 °C, followed by natural cooling. (**c**) Sample matrix, indicating which precursor was sulphurised at which temperature and the codes of the resulting samples.

Table 1. Deposition conditions of the precursor stacks. Rates were measured with the quartz crystal microbalance. RT denotes room temperature (22 to 25 °C).

Precursor	Layer	Target	Substrate T (°C)	RF Power (W)	Rate (nm/s)	Time (s)	Nominal Thickness (nm)
M-RT	W	W	RT	24	0.0051	210	1.07
	Mo	Mo	RT	29	0.0050	214	1.07
S-RT	WS_x	WS_2	RT	15	0.0049	987	4.8
	MoS_x	MoS_2	RT	17	0.0050	956	4.8
M-500	W	W	500	22	0.0049	436	2.14
	Mo	Mo	500	31	0.0050	428	2.14
M-500/RT	W	W	500	22	0.0049	436	2.14
	Mo	Mo	RT	31	0.0050	428	2.14
S-500	WS_x	WS_2	500	16	0.0053	1822	9.6
	MoS_x	MoS_2	500	17	0.0053	1829	9.6
S-500/RT	WS_x	WS_2	500	16	0.0053	1822	9.6
	MoS_x	MoS_2	RT	17	0.0053	1829	9.6

The nominal thickness of each layer in the stacks deposited at room temperature was 1.07 nm for the metallic precursors and 4.8 nm for the sulphide precursors. For depositions at 500 °C the deposition time was doubled, which corresponds to a nominal thickness of 2.14 nm for the metallic layers and 9.6 nm for the sulphide layers. The doubled time compensates for the material re-evaporated from the heated substrate. The thickness of each layer is set by the deposition time at the rate calibrated with the quartz crystal microbalance before deposition, the microbalance being removed during deposition.

2.2. Sulphurisation

Each precursor sample was placed in a graphite box together with 25 mg of elemental sulphur (99.95%, Sigma-Aldrich, Darmstadt, Germany), as described previously [22,25,26]. The box was closed with a graphite lid and placed at the centre of a horizontal tube furnace (GSL-1600X, MTI Corporation, Richmond, CA, USA) inside a fused-quartz tube with an inner diameter of 50 mm. Alumina plugs were placed inside the quartz tube on both sides of the graphite box. Before heating, the tube was purged with Ar. In contrast to our earlier study [22], in which the tube was back-filled with Ar to 900 Torr, no Ar overpressure was applied, and the gas outlet was left open through a bubbler. The furnace was heated at 10 °C/min to the hold temperature and kept there for 15 min. After the hold, the furnace was switched off and the samples cooled naturally to room temperature at the furnace centre, with a low Ar flow started during cooling.

The two room-temperature precursors were sulphurised at 500, 550, 600, 650 and 700 °C, which produced the series Sm1.1 to Sm1.5 for the metallic precursor M-RT and Ss1.1 to Ss1.5 for the sulphide precursor S-RT. The four precursors deposited with at least one layer at 500 °C were sulphurised at 650 °C. After sulphurisation, these four samples retain the code of their precursor, and the text states whether the precursor or the sulphurised film is meant. The temperature profiles are shown in Figure 1b, and the sample matrix with the sample codes in Figure 1c.

2.3. Characterisation

X-ray reflectivity (XRR) was measured on a Rigaku SmartLab diffractometer (Rigaku Corporation, Tokyo, Japan) with a Cu Kα source and a HyPix-3000 detector in 0D mode. The thickness, mass density and roughness of each layer were obtained by fitting the

measured curves with the LEPTOS software, version 4.01 (Bruker AXS GmbH, Karlsruhe, Germany), for the room-temperature series and the M-500 precursor. The other samples deposited at 500 °C were fitted with a Parratt recursion model [28] with Névot-Croce interface roughness [29], using the same layer models, linear density gradients within the layers where needed, and atomic scattering factors at 8.04 keV from [30]. With the layer parameters of the LEPTOS fits, this model reproduced the measured curves of the eight room-temperature films within their noise, for Sm1.4 above 1.0°, below which its measured curve is flat, so that both programmes calculate the same reflectivity from the same layer model, and free fits with this model returned the same layer thicknesses within 0.3 nm. Each fit was repeated from eight random starting points, and a division of the thickness between layers is reported only where the equally good fits agreed on it. The fitted curves shown in Figure 2 are those of the LEPTOS output, over the angular range used in each fit. The total thickness of every film, and of the films that could not be fitted, was also obtained from the period of the interference fringes by Fourier transformation of the reflectivity multiplied by q^4 against the refraction-corrected scattering vector, with the critical scattering vector varied between 0.030 and 0.050 $Å^{-1}$. The total thickness is given as the centre of the values obtained over this range ± half their spread. The Fourier method reproduced the fitted total thickness of the room-temperature films within 0.3 nm. X-ray diffraction (XRD) in the Bragg–Brentano geometry and grazing incidence XRD (GIXRD) were measured on an Anton Paar XRDynamic 500 diffractometer (Anton Paar GmbH, Graz, Austria) with Cu Kα radiation (λ = 1.54187 Å) and a Pixos 2000 detector. GIXRD was acquired at an incidence angle of 0.2°. The position, integral breadth and area of the 002 reflection were obtained by fitting, and the mean crystallite size perpendicular to the substrate was calculated from the integral breadth with the Scherrer equation. For the series deposited at 500 °C, and for Sm1.4 and Ss1.4 used as references, the 002 reflection was fitted with a pseudo-Voigt function and a linear background between 10 and 18°, and the crystallite size was calculated with a shape factor of 1. The instrumental breadth, below 0.21° from the Si substrate reflection near 33°, was not subtracted. The reference positions of the 002 reflection, 14.390° for 2H-MoS_2 and 14.332° for 2H-WS_2, were calculated for λ = 1.54187 Å from the d-spacings of the powder diffraction file, 6.1554 Å (PDF 00-037-1492) and 6.1800 Å (PDF 00-008-0237), as in [22].

Micro-Raman spectra were recorded in backscattering geometry on a LabRAM HR Evolution spectrometer (HORIBA Jobin Yvon, Palaiseau, France) with a confocal microscope, using excitation wavelengths of 532 nm and 633 nm. The precursors deposited at 500 °C were measured with a 50× long working distance objective and an 1800 lines/mm grating, with neutral density filters transmitting 3.2% or 5% of the laser power at 532 nm and 10% or 5% at 633 nm. The room-temperature series were measured at 532 nm only, on a second LabRAM HR Evolution spectrometer, with a 50× objective, a 600 lines/mm grating and a neutral density filter transmitting 5% of the laser power, with 15 accumulations of 15 s or 20 accumulations of 20 s. The Raman shift in each spectrum was corrected so that the Si band is at 519.8 cm^{-1}. On each sample of the hot-substrate series, spectra were recorded at several positions in the centre and near the edge of the 20 mm × 15 mm substrate, at both wavelengths, at different points for the two wavelengths. Spectra were normalised to the Si peak for comparison between samples at the same wavelength. Because the two gratings differ in resolution, band widths are compared only within each series. Spectra at 532 nm were fitted with a linear background and five Lorentzian components (WS_2 2LA(M), WS_2 $E^1{}_{2g}$, MoS_2 $E^1{}_{2g}$, MoS_2-like A_{1g} and WS_2-like A_{1g}), between 325 and 445 cm^{-1} for the room-temperature series and between 335 and 445 cm^{-1} for the series deposited at 500 °C. For the comparison of the two wavelengths, the spectra of the films sulphurised at 650 °C were fitted between 335 and 480 cm^{-1} with a linear background and six Lorentzian components

(WS_2 2LA(M), WS_2 E^1_{2g}, MoS_2 E^1_{2g}, MoS_2-like A_{1g}, the band at 416 to 420 cm^{-1} and the band at 445 to 460 cm^{-1}), and band intensities were compared as ratios of integrated areas within each spectrum.

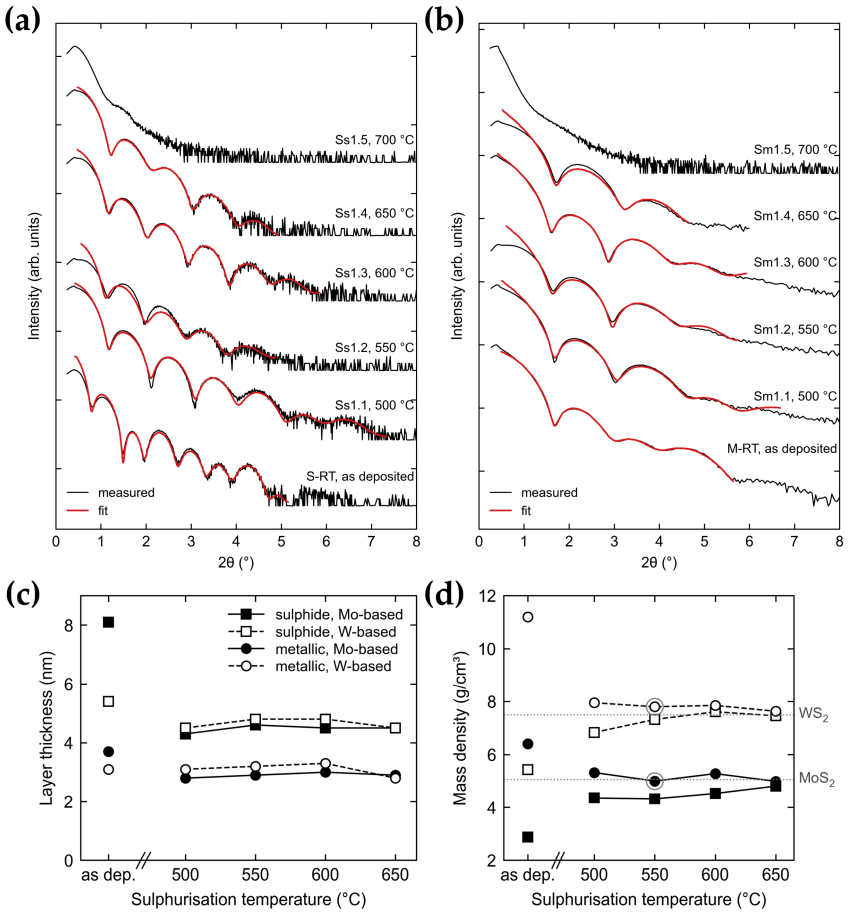


Figure 2. X-ray reflectivity of the room-temperature precursors after sulphurisation. (**a**) Measured XRR curves (black) of the as-deposited S-RT precursor and of the sulphide series Ss1.1 to Ss1.5, vertically offset, with the curves calculated from the fitted parameters (red) over the angular range of each fit. Ss1.5 could not be fitted. (**b**) The same for the M-RT precursor and the metallic series Sm1.1 to Sm1.5. Sm1.5 could not be fitted. (**c**) Thickness of the Mo-based and W-based layers against sulphurisation temperature for both series, with the as-deposited values at the left. (**d**) Mass density of the Mo-based and W-based layers against sulphurisation temperature, with the bulk densities of MoS_2 and WS_2 as dotted lines. The densities of Sm1.2 (ringed) are approximate.

Scanning electron microscopy (SEM) was carried out on a Zeiss EVO 50 XVP microscope (Carl Zeiss NTS, Oberkochen, Germany) with a LaB_6 cathode. Images were recorded with a secondary electron detector in high vacuum (approximately 10^{-6} mbar), at accelerating voltages of 5 to 20 kV, working distances of 9 to 12.5 mm and magnifications from 1000× to 30,000×.

2.4. Use of Generative Artificial Intelligence

During manuscript preparation, a generative AI tool (Claude Opus 5.5, Anthropic, San Francisco, CA, USA, accessed through the Claude Code interface) was used to support the literature-search process by identifying potentially relevant publications and assisting in the compilation of candidate references. It was also used to cross-check the consistency of the information presented across the manuscript. The AI-assisted outputs were treated

as preliminary suggestions and were independently evaluated by the authors before being incorporated into the manuscript.

3. Results

3.1. Precursor Stacks Deposited at Room Temperature

The as-deposited precursors were characterised by XRR and Raman spectroscopy. The layer thicknesses obtained from the XRR fits are well above the nominal values for both precursors (Table 2). The Mo-based layer of M-RT was 3.7 nm thick with a density of 6.4 g/cm^3, against 1.07 nm and 10.22 g/cm^3 for metallic Mo, and the W-based layer was 3.1 nm thick with a density of 11.2 g/cm^3, against 1.07 nm and 19.25 g/cm^3 for metallic W. The fit of the sulphide precursor S-RT resulted in 8.1 nm at 2.88 g/cm^3 for the MoS_x layer and 5.4 nm at 5.43 g/cm^3 for the WS_x layer, against a nominal 4.8 nm for each. GIXRD of both precursors showed no reflections of MoS_2, WS_2, Mo or W, only the broad halo of the amorphous SiO_2 substrate near 21° (Section 3.3), and neither precursor showed Raman bands in the 300 to 460 cm^{-1} range (Section 3.4). Both precursors were therefore amorphous before sulphurisation.

Table 2. Thickness (t), mass density (ρ) and areal mass (t·ρ) of the Mo-based and W-based layers from XRR. Bulk densities are 10.22 g/cm^3 (Mo), 19.25 g/cm^3 (W), 5.06 g/cm^3 (MoS_2) and 7.5 g/cm^3 (WS_2). At 700 °C no fit was possible.

Sample	T (°C)	t Mo-Based (nm)	ρ Mo-Based (g/cm^3)	t·ρ Mo-Based (nm·g/cm^3)	t W-Based (nm)	ρ W-Based (g/cm^3)	t·ρ W-Based (nm·g/cm^3)	t Total (nm)
S-RT precursor	-	8.1	2.88	23.3	5.4	5.43	29.3	13.5
Ss1.1	500	4.3	4.36	18.7	4.5	6.83	30.7	8.8
Ss1.2	550	4.6	4.33	19.9	4.8	7.32	35.1	9.4
Ss1.3	600	4.5	4.53	20.4	4.8	7.61	36.5	9.3
Ss1.4	650	4.5	4.81	21.6	4.5	7.46	33.6	9.0
Ss1.5	700	-	-	-	-	-	-	-
M-RT precursor	-	3.7	6.4	23.7	3.1	11.2	34.7	6.8
Sm1.1	500	2.8	5.32	14.9	3.1	7.95	24.6	5.9
Sm1.2	550	2.9	~5.0	~14.5	3.2	~7.8	~25.0	6.1
Sm1.3	600	3.0	5.28	15.8	3.3	7.85	25.9	6.3
Sm1.4	650	2.9	4.99	14.5	2.8	7.63	21.4	5.7
Sm1.5	700	-	-	-	-	-	-	-

3.2. Thickness and Density After Sulphurisation

The XRR curves of both series showed interference fringes up to 650 °C (Figure 2a,b), and they were fitted with two-layer models. After sulphurisation at 700 °C, the fringes were strongly damped and no fit was possible for either series, which indicates a rough or laterally non-uniform film. The fitted thicknesses and densities are given in Table 2 and plotted against temperature in Figure 2c,d.

In the sulphide series, the Mo-based layer was 4.3 to 4.6 nm thick and the W-based layer 4.5 to 4.8 nm thick between 500 and 650 °C, for a total of 8.8 to 9.4 nm. The density of the Mo-based layer increased from 4.36 g/cm^3 at 500 °C to 4.81 g/cm^3 at 650 °C, below the bulk MoS_2 value of 5.06 g/cm^3. The density of the W-based layer increased from 6.83 g/cm^3 at 500 °C to 7.61 g/cm^3 at 600 °C, close to the bulk WS_2 value of 7.5 g/cm^3. The total areal mass of the two layers, the product of thickness and density summed over both, was 94 to 108% of that of the precursor. The Mo-based layer retained 80 to 93% of the areal mass of the MoS_x precursor, while the W-based layer reached 105 to 125% of the areal mass of the WS_x precursor.

In the metallic series, the Mo-based layer was 2.8 to 3.0 nm thick and the W-based layer 2.8 to 3.3 nm thick between 500 and 650 °C, for a total of 5.7 to 6.3 nm. The density of the Mo-based layer was 4.99 to 5.32 g/cm^3, close to bulk MoS_2, and that of the W-based layer was 7.63 to 7.95 g/cm^3, slightly above bulk WS_2. From the bulk molar volumes, complete sulphurisation of the nominal 1.07 nm metal layers would result in 3.6 nm of MoS_2 and 3.7 nm of WS_2. The measured thicknesses are 76 to 89% of these values, and the total areal mass is 78 to 91% of that of these disulphide layers. Both series reached their largest total thickness at 550 or 600 °C and were thinner at 650 °C.

3.3. Crystal Structure

The GIXRD patterns of the as-deposited precursors contained no reflections, while those of the sulphurised films showed the 002 reflection of the hexagonal disulphides near 14° in both series (Figure 3a,b). The sulphide precursor sulphurised at 500 °C (Ss1.1) showed, in addition, weak reflections between 20 and 24° and near 33° that are assigned to a Mo-W oxide (Figure 3a). No oxide reflections were detected in the metallic series (Figure 3b). In the Bragg–Brentano geometry, only the 002 reflection was observed between 500 and 650 °C in both series, while the films sulphurised at 700 °C also showed the 004, 006 and 008 reflections (Figure 3c,d). The films are therefore strongly textured with the basal planes parallel to the substrate.

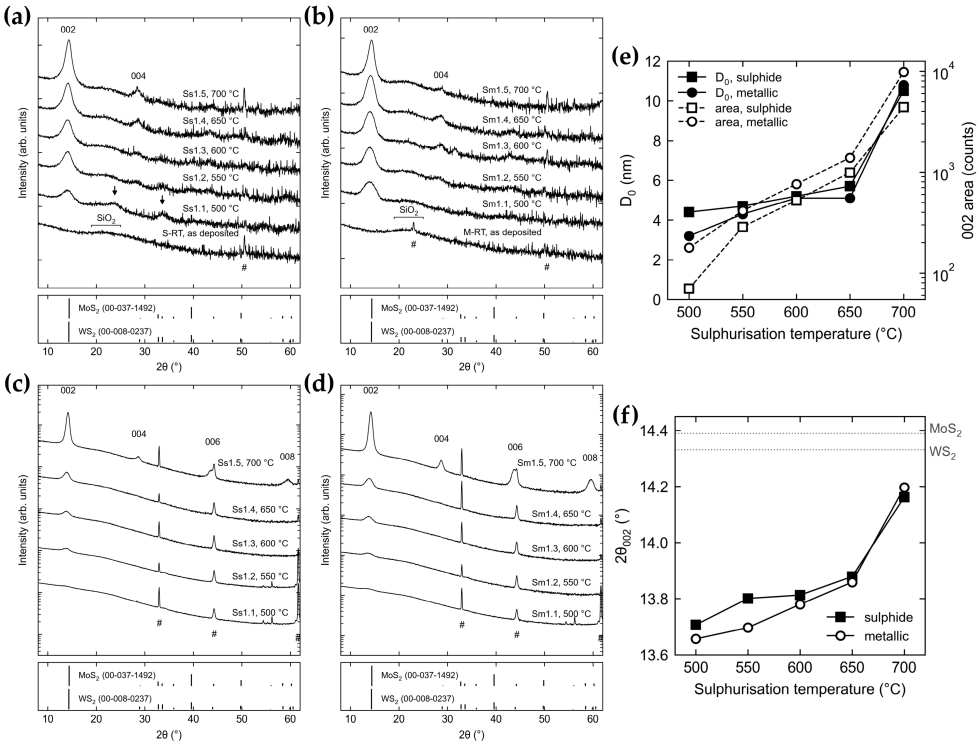


Figure 3. X-ray diffraction of the room-temperature precursors after sulphurisation. (**a**) GIXRD patterns of the sulphide precursor as deposited and of Ss1.1 to Ss1.5, with the reflections of the Mo-W oxide of Ss1.1 indicated by arrows. (**b**) GIXRD patterns of the metallic precursor as deposited and of Sm1.1 to Sm1.5. (**c**) Bragg–Brentano XRD patterns of the sulphide series. (**d**) Bragg–Brentano XRD patterns of the metallic series. In (**a**–**d**) the patterns are vertically offset, the halo of the amorphous SiO_2 substrate is labelled, # denotes narrow lines that do not belong to the films, and the reference positions of 2H-MoS_2 (PDF 00-037-1492) and 2H-WS_2 (PDF 00-008-0237) are shown at the bottom. (**e**) Mean crystallite size D_0 (filled symbols) and area of the 002 reflection (open symbols) against sulphurisation temperature. (**f**) Position of the 002 reflection against sulphurisation temperature for both series, with the reference positions of 2H-MoS_2 and 2H-WS_2 as dotted lines.

The parameters of the 002 reflection are given in Table 3. The area of the 002 reflection increased with temperature in both series, by a factor of 14 between 500 and 650 °C for the sulphide series and by a factor of 8 for the metallic series, and by a further factor of 4 to 7 at 700 °C. The mean crystallite size perpendicular to the substrate, D_0, increased from 4.4 to 5.7 nm (sulphide) and from 3.2 to 5.1 nm (metallic) between 500 and 650 °C (Figure 3e). At 700 °C, D_0 reached 10.5 and 10.8 nm, larger than the mean film thickness measured at lower temperatures.

Table 3. Parameters of the 002 reflection in the Bragg–Brentano XRD. β is the integral breadth, D_0 the mean crystallite size perpendicular to the substrate from the Scherrer equation with a shape factor of 1, and t the total thickness from XRR.

Sample	T (°C)	Area (Counts)	β (° 2θ)	D_0 (nm)	t (nm)	$2\theta_{002}$ (°)
Ss1.1	500	70	2.013	4.4	8.8	13.707
Ss1.2	550	287	1.876	4.7	9.4	13.801
Ss1.3	600	525	1.712	5.2	9.3	13.813
Ss1.4	650	990	1.567	5.7	9.0	13.879
Ss1.5	700	4404	0.847	10.5	-	14.162
Sm1.1	500	178	2.749	3.2	5.9	13.657
Sm1.2	550	415	2.077	4.3	6.1	13.697
Sm1.3	600	760	1.760	5.1	6.3	13.780
Sm1.4	650	1387	1.762	5.1	5.7	13.859
Sm1.5	700	9833	0.824	10.8	-	14.197
Reference 2H-MoS_2						14.390
Reference 2H-WS_2						14.332

The 002 reflection of all sulphurised films was located below the reference positions of both 2H-MoS_2 (14.390°) and 2H-WS_2 (14.332°) [22]. The 002 reflection moved from 13.707° to 13.879° (sulphide) and from 13.657° to 13.859° (metallic) between 500 and 650 °C, and reached 14.162° and 14.197° at 700 °C (Figure 3f). The two reference positions differ by 0.058°, which is 2 to 7% of the integral breadth of the reflection (0.8 to 2.7°), so the position of the 002 reflection cannot distinguish MoS_2, WS_2 and their alloys in the sulphurised films. The shift toward the reference positions occurred together with the increase in D_0.

3.4. Raman Spectra at 532 nm

The Raman spectra recorded at 532 nm before and after sulphurisation are shown in Figure 4a,b. Each spectrum was fitted with the five Lorentzian components described in Section 2.3, as in [22]. The fitted positions, averaged over three positions on each sample, are given in Table 4 and plotted in Figure 4c,d. The standard deviation between positions on the same sample was 0.3 cm^{-1} or less for all A_{1g} components below 700 °C, except the weak WS_2-like component of Ss1.1 (0.4 cm^{-1}). The standard errors of the fitted A_{1g} positions were 0.1 to 0.6 cm^{-1}, except for the weak WS_2-like component of Ss1.1. At 700 °C the standard deviation between positions of the MoS_2-like band of Sm1.5 was 0.56 cm^{-1}.

After sulphurisation at 500 °C, the metallic precursor (Sm1.1) showed the bands of both MoS_2 and WS_2. The sulphide precursor (Ss1.1) showed the $E^1{}_{2g}$ and A_{1g} bands of MoS_2 at 380.6 and 406.8 cm^{-1}, while the WS_2 bands were nearly absent (Figure 4a). Only a weak component near 412 cm^{-1} was fitted on the high-frequency side of the MoS_2 A_{1g} band. From 550 °C both series showed all five components.

Between 550 and 650 °C the spectra of both series contained two separate A_{1g} bands. The MoS_2-like A_{1g} was located at 407.3 to 407.8 cm^{-1}, close to the value of 407.4 cm^{-1} reported for bulk MoS_2 [31]. The WS_2-like A_{1g} was located at 416.7 to 417.6 cm^{-1}, 2.5 to 3.4 cm^{-1} below the value of 420.1 cm^{-1} for bulk WS_2 at 514.5 nm and close to the value

reported for monolayer and bilayer WS_2 [32]. The separation between the two A_{1g} bands was 9.3 to 9.7 cm^{-1} in the metallic series and 9.8 to 10.3 cm^{-1} in the sulphide series. In the metallic film sulphurised at 500 °C, the WS_2-like A_{1g} was located at 415.6 cm^{-1}, 1.1 cm^{-1} lower than at 550 °C, and the separation was 8.4 cm^{-1}. The intensity of the 2LA(M) band of WS_2 exceeded that of the WS_2-like A_{1g} in both series between 550 and 650 °C, with ratios of 1.0 to 1.7.

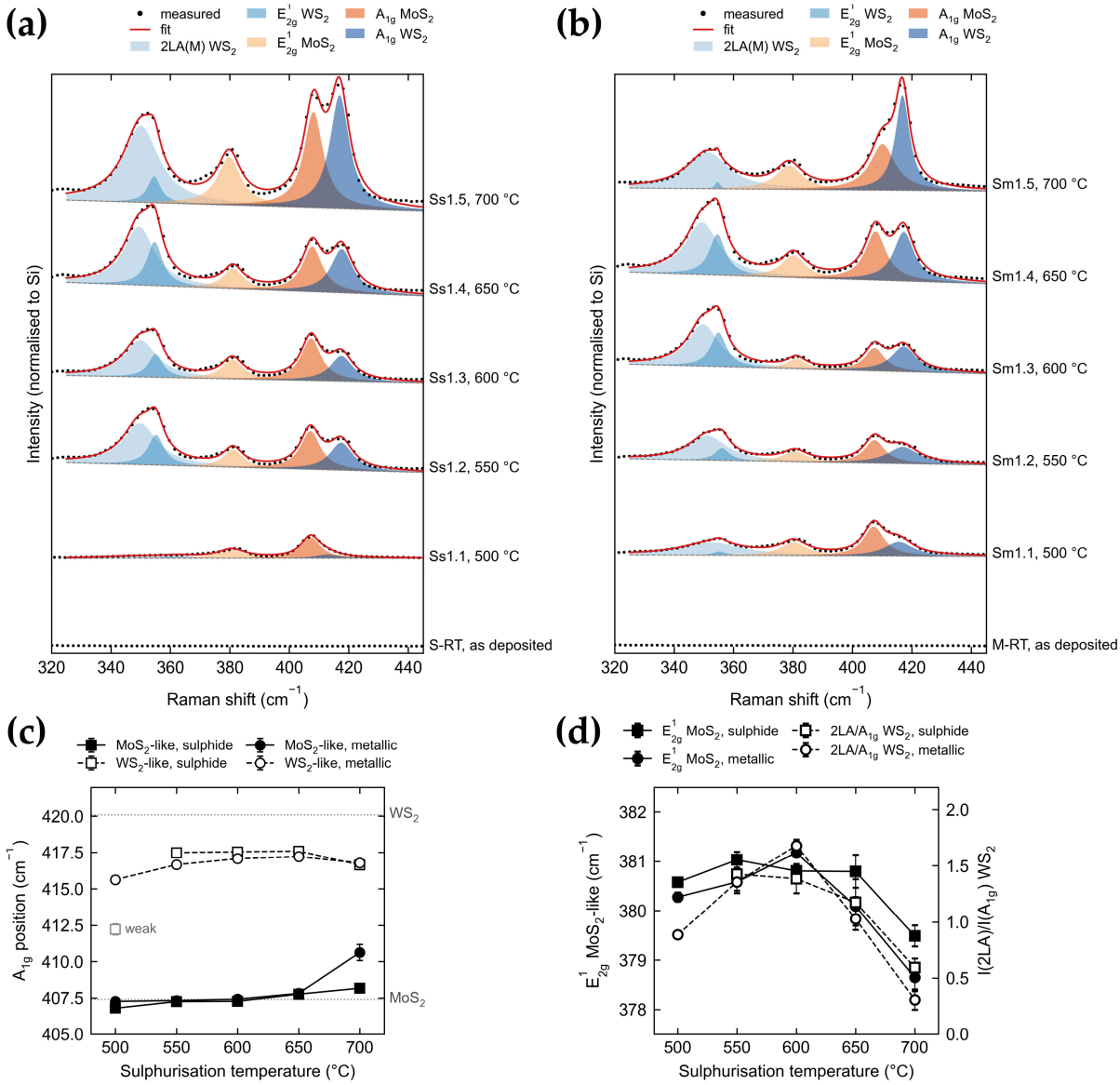


Figure 4. Raman spectra at 532 nm of the room-temperature precursors before and after sulphurisation. (**a**) Spectra (points) of the sulphide precursor as deposited and of Ss1.1 to Ss1.5 at one position, normalised to the Si band and vertically offset, with the five-component Lorentzian fits (red), their components (filled, WS_2 bands in blue and MoS_2 bands in orange) and the linear background (dashed). The precursor shows no bands and is not fitted. (**b**) The same for the metallic precursor and Sm1.1 to Sm1.5. (**c**) Positions of the MoS_2-like (filled symbols) and WS_2-like (open symbols) A_{1g} bands against sulphurisation temperature for both series, with the bulk values of MoS_2 (407.4 cm^{-1}) and WS_2 (420.1 cm^{-1}) as dotted lines. The weak WS_2-like band of Ss1.1 is shown in grey. (**d**) Position of the MoS_2-like $E^1{}_{2g}$ band (filled symbols) and ratio of the 2LA(M) to A_{1g} intensities of WS_2 (open symbols) against sulphurisation temperature, the ratio not given for Ss1.1. In (**c**,**d**) the values are the mean of three positions and the error bars their standard deviation.

Table 4. Raman band positions at 532 nm from five-component Lorentzian fits, mean of three positions per sample. Δ is the separation between the WS_2-like and MoS_2-like A_{1g} bands, and I(2LA)/I(A_{1g}) the ratio of the fitted peak intensities of the WS_2 2LA(M) and A_{1g} bands.

Sample	T (°C)	E^1_{2g} MoS_2 (cm^{-1})	A_{1g} MoS_2-like (cm^{-1})	A_{1g} WS_2-like (cm^{-1})	Δ (cm^{-1})	I(2LA)/I(A_{1g}) WS_2
Ss1.1	500	380.6	406.8	412.2 (weak)	-	-
Ss1.2	550	381.0	407.3	417.5	10.2	1.4
Ss1.3	600	380.8	407.3	417.5	10.3	1.4
Ss1.4	650	380.8	407.8	417.6	9.8	1.2
Ss1.5	700	379.5	408.2	416.7	8.5	0.6
Sm1.1	500	380.3	407.3	415.6	8.4	0.9
Sm1.2	550	380.6	407.3	416.7	9.3	1.4
Sm1.3	600	381.2	407.4	417.1	9.7	1.7
Sm1.4	650	380.1	407.8	417.2	9.4	1.0
Sm1.5	700	378.6	410.6	416.8	6.2	0.3

At 700 °C, the two A_{1g} bands moved toward each other in both series (Figure 4c). In the metallic series, the MoS_2-like A_{1g} shifted from 407.8 to 410.6 cm^{-1}, the WS_2-like A_{1g} from 417.2 to 416.8 cm^{-1}, and the separation decreased from 9.4 to 6.2 cm^{-1}, with a propagated fit uncertainty of 0.6 cm^{-1}. In the sulphide series, the MoS_2-like A_{1g} shifted from 407.8 to 408.2 cm^{-1} and the separation decreased from 9.8 to 8.5 cm^{-1}. The MoS_2-like E^1_{2g} band shifted to lower wavenumber, from 380.1 to 378.6 cm^{-1} (metallic) and from 380.8 to 379.5 cm^{-1} (sulphide) (Figure 4d). The ratio of the 2LA(M) to A_{1g} intensities of WS_2 decreased to 0.3 (metallic) and 0.6 (sulphide). A displacement of the MoS_2-like and WS_2-like A_{1g} bands toward each other has been reported as W and Mo mix on the metal sublattice of $Mo_{1-x}W_xS_2$ [33,34].

Raman spectra probe the positions of the A_{1g} bands averaged over the laser spot and through the film thickness. Mixing is inferred here from the convergence of the two A_{1g} bands, and the vertical distribution of Mo and W was not measured. No Raman bands of MoO_3 or WO_3 were detected between 650 and 1000 cm^{-1} in any sample.

3.5. Precursors Deposited at 500 °C

The four precursors deposited with at least one layer at 500 °C (M-500, M-500/RT, S-500 and S-500/RT) were sulphurised at 650 °C, the highest temperature at which the XRR curves of the room-temperature films could still be fitted (Section 3.2). These four samples are compared below with the room-temperature precursors sulphurised under the same conditions, Sm1.4 and Ss1.4.

3.5.1. Thickness and Structure of the Precursors

The XRR curves of the four precursors are shown in Figure 5a, and the total thickness obtained from the period of their interference fringes (Figure 5c) is given in Table 5. The M-500 precursor was 4.0 ± 0.2 nm thick, thinner than its nominal metal thickness of 4.28 nm, as was M-500 after sulphurisation (Section 3.5.2). The curve of the M-500/RT precursor contained two periods, corresponding to a dominant component of 3.0 nm and a weak component of 9 nm (Figure 5c). The fitted layer parameters are given in Table 6. The M-500 precursor consisted of 1.19 nm of W (18.1 g/cm^3) and 1.53 nm of Mo (9.5 g/cm^3) under a 1.96 nm oxide layer. The fit of the M-500/RT precursor contained 2.3 nm of W (17.5 g/cm^3) under 7.1 nm of oxide with a density of 4.5 g/cm^3, close to that of MoO_3 (4.70 g/cm^3), with at most 0.6 nm of a denser layer (6.0 g/cm^3) between them. Complete oxidation of the nominal 2.14 nm of Mo to MoO_3 would result in 7.0 nm, from the bulk molar volumes. A model without any Mo layer described the M-500/RT curve only slightly

less well, whereas removing the Mo layer of M-500 clearly degraded its fit. The results are therefore consistent with full oxidation of the Mo layer of M-500/RT, deposited at room temperature on W deposited at 500 °C, while the Mo layer of M-500, deposited at 500 °C, remained partly metallic.

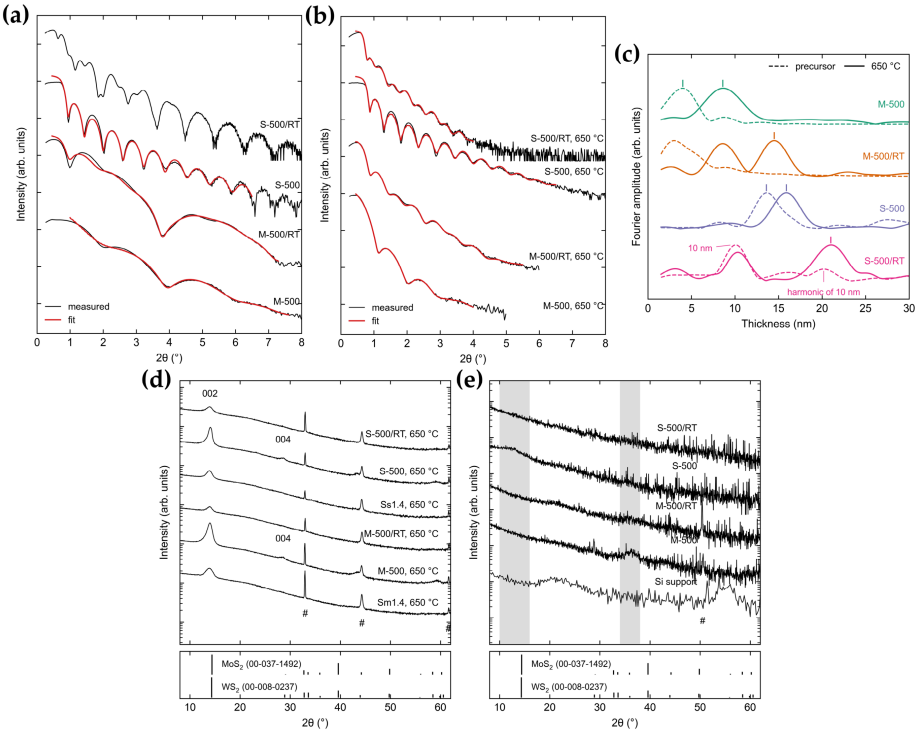


Figure 5. X-ray reflectivity and diffraction of the precursors deposited at 500 °C. (**a**) Measured XRR curves (black) of the M-500, M-500/RT, S-500 and S-500/RT precursors, vertically offset, with the curves calculated from the fitted parameters (red) over the angular range of each fit. The S-500/RT precursor could not be fitted. (**b**) The same for the four films after sulphurisation at 650 °C. (**c**) Fourier transforms of the curves in (**a**) (dashed) and (**b**) (solid), with the total thicknesses indicated. For the S-500/RT precursor the component near 20 nm is a harmonic of the 10 nm component. (**d**) Bragg–Brentano XRD patterns of the four films sulphurised at 650 °C and of Sm1.4 and Ss1.4. (**e**) GIXRD patterns of the four precursors and of the bare substrate, with the broad features of S-500 and M-500 shaded. In (**d**,**e**) # denotes narrow lines of the substrate, and the reference positions of 2H-MoS_2 (PDF 00-037-1492) and 2H-WS_2 (PDF 00-008-0237) are shown at the bottom.

Table 5. Total thickness from the Fourier transform of the XRR curves, given as the centre ± half the range for critical scattering vectors from 0.030 to 0.050 Å^{-1} (for Sm1.4 and Ss1.4, the totals of the fits in Table 2), and parameters of the 002 reflection in Bragg–Brentano XRD for the precursors deposited at 500 °C, before and after sulphurisation at 650 °C, with the room-temperature precursors sulphurised at 650 °C for comparison. The expected thickness assumes complete sulphurisation of the nominal metal layers. β is the integral breadth and D_0 the mean crystallite size perpendicular to the substrate. The 002 parameters of Sm1.4 and Ss1.4 were refitted with the same procedure as the hot series.

Sample	Nominal (nm)	Expected After Sulphurisation (nm)	Total t, Precursor (nm)	Total t, 650 °C (nm)	$2\theta_{002}$ (°)	β (° 2θ)	D_0 (nm)	Area (Counts·°)
M-500	4.28 (metal)	14.6	4.0 ± 0.2	8.6 ± 0.3	13.943	1.529	5.8	42,371
M-500/RT	4.28 (metal)	14.6	3.0 and 9	14.5 ± 0.2	13.916	1.612	5.5	5458
S-500	19.2	-	13.6 ± 0.2	15.9 ± 0.2	14.042	1.222	7.3	26,177
S-500/RT	19.2	-	not determined [a]	21.0 ± 0.3	13.905	2.127	4.2	8978
Sm1.4 (M-RT)	2.14 (metal)	7.3	6.8	5.7	13.860	1.765	5.0	-
Ss1.4 (S-RT)	9.6	-	13.5	9.0	13.869	1.719	5.2	-

[a] The curve is dominated by a dense layer of 9.8 to 9.9 nm. The component near 20 nm in its Fourier transform is a harmonic of that layer, see the text.

Table 6. Layer thickness t and mean mass density ρ from fits of the XRR curves of the precursors deposited at 500 °C, before and after sulphurisation at 650 °C. Layers are listed from the surface. For M-500/RT and S-500/RT after sulphurisation the layers have linear density gradients and ρ is the mean.

Sample	Layers, t (nm) and ρ (g/cm^3)	Total t (nm)
M-500, precursor	Mo oxide 1.96, 6.2 Mo 1.53, 9.5 W 1.19, 18.1	4.7
M-500/RT, precursor	Mo oxide 7.1, 4.5 Mo-based 0.6, 6.0 W 2.3, 17.5	9.9
S-500, precursor	division between MoS_x and WS_x not determined [b]	14.0–14.2
S-500/RT, precursor	dense layer (WS_x) 9.8–9.9, ≥7.5 MoS_x not resolved	not determined
M-500, 650 °C	division between MoS_2 and WS_2 not determined [b]	8.8–11.0
M-500/RT, 650 °C	MoS_2 9.0, 4.7 WS_2 5.6, 5.2	14.7
S-500, 650 °C	division between MoS_2 and WS_2 not determined [b]	15.7–16.1
S-500/RT, 650 °C	MoS_2 9.8, 5.1 WS_2 11.6, 5.6	21.4

[b] Fits with very different divisions of the total between the two layers described the curve equally well. The range of totals is over these fits.

In the two sulphide precursors, the WS_x layers were deposited under identical conditions, both at 500 °C, and the precursors differ only in the substrate temperature during the deposition of the MoS_x layer. The S-500 precursor, with MoS_x deposited at 500 °C, was 13.6 ± 0.2 nm thick, against a nominal 19.2 nm. The curve of the S-500/RT precursor, with MoS_x deposited at room temperature, was dominated by a single fringe period corresponding to 10.0 to 10.2 nm (Figure 5a,c). The Fourier transform of this curve also contained a component near 20 nm. A single dense layer of 9.9 nm with sharp interfaces reproduces both components with the same relative amplitudes, so the 20 nm component is a harmonic of the first and not a second thickness. No model with up to three layers, nor one with partial coverage by the MoS_x layer, described this curve, but every fit contained a dense layer of 9.8 to 9.9 nm with a roughness of 0.35 nm. The dense layer is attributed to the WS_x deposited at 500 °C (nominal 9.6 nm). The MoS_x layer deposited at room temperature contributed little to the specular reflectivity, consistent with the low density of the MoS_x deposited at room temperature in the S-RT precursor (2.9 g/cm^3, Table 2) and with the particles of 10 to 30 nm on the surface of the S-500/RT precursor (Section 3.5.4). The total thickness of the S-500/RT precursor could therefore not be determined by XRR, and the two sulphide films are compared after sulphurisation (Section 3.5.2).

The GIXRD patterns of the four precursors contained no sharp reflections (Figure 5e). The S-500 precursor showed a broad feature between 10 and 16°, near the position of the 002 reflection of the disulphides, which was absent from S-500/RT. The M-500 precursor showed a broad feature between 34 and 38°. No Raman bands were detected at 532 nm in either sulphide precursor.

3.5.2. Thickness and Structure After Sulphurisation

After sulphurisation at 650 °C, M-500 was 8.6 ± 0.3 nm thick and M-500/RT was 14.5 ± 0.2 nm thick (Figure 5b,c and Table 5). Complete sulphurisation of the nominal metal layers, calculated from the bulk molar volumes as in Section 3.2, would result in

14.6 nm thickness for both M-500 and M-500/RT. The measured thickness is therefore 59 ± 2% of this value for M-500 and 99 ± 2% for M-500/RT.

After sulphurisation, the two sulphide films were 15.9 ± 0.2 nm (S-500) and 21.0 ± 0.3 nm (S-500/RT) thick. Since their WS_x layers were deposited under the same conditions, the difference of 5.1 ± 0.5 nm is attributed to the MoS_x layer, which remained on the substrate in a smaller amount when it was deposited at 500 °C. S-500 became thicker during sulphurisation, from 13.6 ± 0.2 to 15.9 ± 0.2 nm, whereas the sulphide precursor deposited entirely at room temperature (S-RT) became thinner, from 13.5 to 9.0 nm at 650 °C (Table 5).

Fits with a two-layer MoS_2/WS_2 model reproduced these totals within 0.7 nm for M-500/RT, S-500 and S-500/RT, and resulted in 8.8 to 11.0 nm for M-500, depending on the model (Table 6). For M-500/RT and S-500/RT, linear density gradients in both layers, as in the fits of the room-temperature films, described the curves clearly better than uniform layers. The fits with density gradients contained MoS_2 and WS_2 layers of 9.0 and 5.6 nm for M-500/RT and of 9.8 and 11.6 nm for S-500/RT, with mean densities of 4.7 to 5.2 g/cm^3 for MoS_2 and 5.2 to 5.6 g/cm^3 for WS_2, below the bulk values (5.06 and 7.5 g/cm^3) in the case of WS_2. For M-500 and S-500, fits with very different divisions of the total between the two layers described the data equally well, and only the total thickness is given.

All four sulphurised films showed the 002 reflection of the hexagonal disulphides in both GIXRD and the Bragg–Brentano geometry, and M-500 and S-500 also showed the 004 reflection near 28.6° (Figure 5d). The parameters of the 002 reflection in the Bragg–Brentano geometry are given in Table 5. As in the room-temperature series, the 002 reflection was below the reference positions of 2H-MoS_2 and 2H-WS_2, between 13.905 and 14.042°. S-500 had the highest 002 position and the largest crystallite size, D_0 = 7.3 nm, and S-500/RT the smallest, 4.2 nm. The crystallite size of M-500 and M-500/RT was 5.8 and 5.5 nm, against 5.0 and 5.2 nm for Sm1.4 and Ss1.4 fitted in the same way. The four hot-series films were measured under identical conditions, so the areas of their 002 reflections can be compared directly. The area was largest for M-500 and eight times smaller for M-500/RT, although M-500/RT is the thicker film. The GIXRD patterns of S-500 and M-500 contained weak additional reflections near 18.6°, and that of S-500 a further one near 23.2°, which were not assigned.

3.5.3. Raman Spectra at 532 nm, Centre and Edge

The Raman spectra of the four sulphurised films are shown in Figure 6a,b, and the fitted positions of the two A_{1g} bands at each measured position are given in Table 7 and Figure 6c. The spectra varied strongly between positions on the same film, so the positions are reported individually and not averaged.

In the two metallic films, the spectra contained the bands of both disulphides at every position. At the centre of the samples, the separation between the MoS_2-like and WS_2-like A_{1g} bands was 9.0 to 10.2 cm^{-1}, as in Sm1.4 and Ss1.4 (Table 4). Near the edges, the separation decreased to 5.4 to 7.4 cm^{-1}. Averaged over each zone, the MoS_2-like band was 1.7 to 1.9 cm^{-1} higher at the edge and the WS_2-like band 0.7 cm^{-1} (M-500/RT) to 2.4 cm^{-1} (M-500) lower. The same displacement of the two A_{1g} bands toward each other was found for the room-temperature metallic precursor after sulphurisation at 700 °C (Sm1.5, separation 6.2 cm^{-1}, Section 3.4), and it was reported for the mixing of W and Mo on the metal sublattice [33,34]. In the metallic films deposited at 500 °C, this displacement was observed at 650 °C, but only near the edges.

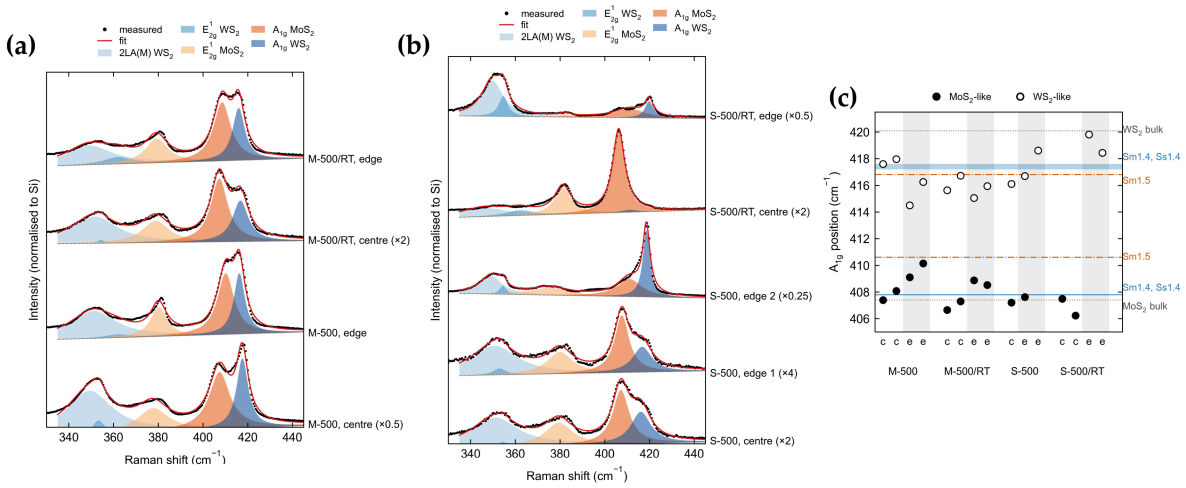


Figure 6. Raman spectra at 532 nm of the precursors deposited at 500 °C after sulphurisation at 650 °C. (**a**) Spectra (points) of M-500 and M-500/RT at the centre and near the edge of the samples, normalised to the Si band, scaled by the factors given and vertically offset, with the five-component Lorentzian fits (red), their components (filled, WS_2 bands in blue and MoS_2 bands in orange) and the linear background (dashed). (**b**) The same for S-500 and S-500/RT. (**c**) Positions of the MoS_2-like (filled) and WS_2-like (open) A_{1g} bands at each measured position, centre (c) and edge (e, shaded), with the values of Sm1.4 and Ss1.4 (blue), of Sm1.5 (orange, dash-dotted) and the bulk values of MoS_2 (407.4 cm^{-1}) and WS_2 (420.1 cm^{-1}) (dotted) for comparison. MoS_2-like bands that appear only as a shoulder and WS_2-like bands too weak to fit are not plotted in (**c**).

Table 7. Raman band positions at 532 nm of the films sulphurised at 650 °C, from five-component Lorentzian fits at each measured position. Δ is the separation between the WS_2-like and MoS_2-like A_{1g} bands, and I(W)/I(Mo) the ratio of their fitted peak intensities.

Sample	Position	A_{1g} MoS_2-like (cm^{-1})	A_{1g} WS_2-like (cm^{-1})	Δ (cm^{-1})	I(W)/I(Mo)
M-500	centre 1	407.4	417.6	10.2	1.23
	centre 2	408.1	418.0	9.9	1.17
	edge 1	409.1	414.5	5.4	0.70
	edge 2	410.1	416.3	6.1	1.00
M-500/RT	centre 1	406.7	415.6	9.0	0.20
	centre 2	407.3	416.7	9.4	0.65
	edge 1	408.9	415.1	6.2	0.75
	edge 2	408.5	415.9	7.4	0.89
S-500	centre	407.2	416.1	8.9	0.59
	edge 1	407.6	416.7	9.1	0.44
	edge 2	shoulder	418.6	-	WS_2-dominated
S-500/RT	centre 1	407.5	-	-	0.07
	centre 2	406.2	-	-	0.03
	edge 1	shoulder	419.8	-	WS_2-dominated
	edge 2	shoulder	418.4	-	WS_2-dominated

The sulphide films showed no such displacement. Where both A_{1g} bands were present, their separation was 8.9 to 9.1 cm^{-1}. Instead, the relative intensity of the two components changed from one position to another. At the two centre positions on S-500/RT, the spectra were nearly pure MoS_2-like, with the E^1_{2g} and A_{1g} bands at 381.2 to 382.3 and 406.2 to 407.5 cm^{-1} and a WS_2-like A_{1g} band with a peak intensity of 3 to 7% of that of the MoS_2-like one. The two edge positions on S-500/RT and one near the edge of S-500 were dominated by WS_2, with a narrow A_{1g} band (3.9 to 5.1 cm^{-1} wide) at 418.4 to 419.8 cm^{-1}, closer to the

value of 420.1 cm^{-1} for bulk WS_2 than the WS_2-like band of the other positions [32]. The sulphide films therefore did not show the A_{1g} convergence at 650 °C, but their composition varied laterally on the scale of the separation between the measured positions.

3.5.4. Surface Morphology

SEM images of the precursors and the sulphurised films are shown in Figure 7. All four precursors had smooth surfaces (Figure 7a,c,e,g). The surface of the S-500/RT precursor showed many small round particles of 10 to 30 nm (Figure 7g), and that of the M-500 precursor scattered agglomerates (Figure 7a). After sulphurisation at 650 °C, M-500 had a granular surface with grains of a few tens of nanometres (Figure 7b), and M-500/RT a smooth surface with many-faceted and rod-shaped particles 100 to 200 nm long (Figure 7d). The sulphide films remained smooth after sulphurisation, S-500 with a fine and uniform granular texture (Figure 7f) and S-500/RT with scattered elongated particles up to 1 µm long (Figure 7h) and, in other fields, agglomerates of up to 1 µm.

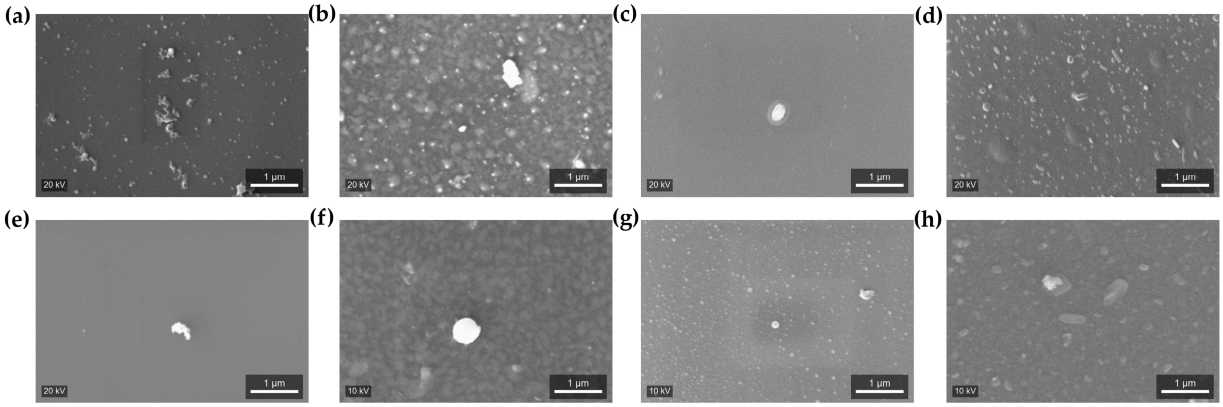


Figure 7. SEM images at 20,000× of the precursors deposited at 500 °C, before and after sulphurisation at 650 °C. (**a**) M-500 precursor before and (**b**) after sulphurisation. (**c**) M-500/RT precursor before and (**d**) after sulphurisation. (**e**) S-500 precursor before and (**f**) after sulphurisation. (**g**) S-500/RT precursor before and (**h**) after sulphurisation. Scale bar 1 µm. The beam voltage is given in each panel.

3.6. Raman Spectra at 633 nm

The two excitation lines probe different excitonic resonances. At 532 nm (2.33 eV), WS_2 is in resonance with its B exciton, and at 633 nm (1.96 eV) with its A exciton [35,36]. MoS_2 is also resonant near 1.96 eV, where several of its second-order bands are anomalously enhanced while the first-order bands are not [37,38]. The four films sulphurised at 650 °C were therefore also measured at 633 nm, at the centre and near the edge of each sample (Figure 8). The spots measured at the two wavelengths were different points of the same zone, so the two lines are compared zone by zone and not spot by spot. Both sets of spectra were fitted with the same six-component model, and the band parameters are summarised in Table 8. Intensities are compared as ratios of integrated areas within each spectrum, because the intensity of the Si reference band itself depends on the excitation wavelength.

Two changes from 532 to 633 nm were common to all four films. The first concerns the WS_2-like bands. The ratio of the 2LA(M) band near 350 cm^{-1} to the WS_2-like A_{1g} band was 0.83 to 5.72 at 532 nm (median 2.0) and 0.02 to 1.31 at 633 nm (median 0.9). The ratio was lower at 633 nm in every zone, with overlapping ranges only at the edges of M-500/RT and S-500 (Figure 8c). The decrease was largest at the edge of S-500/RT, from 1.70–5.72 at 532 nm to 0.85–0.95 at 633 nm, where the spectra at both lines were dominated by WS_2 and the band near 419 cm^{-1} is narrow, so that the ratio there is not affected by MoS_2 bands. A 2LA(M) band stronger than A_{1g} is known in monolayer WS_2 excited near 2.4 eV, where it

arises from a double-resonance process, and it is not dominant under red excitation [32]. The high 2LA(M)/A_{1g} ratios at 532 nm (Table 8, Figure 8c) therefore reflect resonance and the small thickness of the WS_2-like domains, and are not taken as evidence of alloying. The second change concerns the MoS_2-like bands. A broad band between 445 and 460 cm^{-1} increased strongly relative to the MoS_2-like A_{1g} band, from 0.26 to 1.18 at 532 nm to 1.18 to 7.27 at 633 nm, wherever the MoS_2-like A_{1g} was resolved (Figure 8d). The increase matches the anomalous enhancement at 1.96 eV of the broad, asymmetric second-order band of MoS_2 near 460 cm^{-1} [37,39]. WS_2 has no strong band in this range, so this band corresponds to the MoS_2-like component at 633 nm.

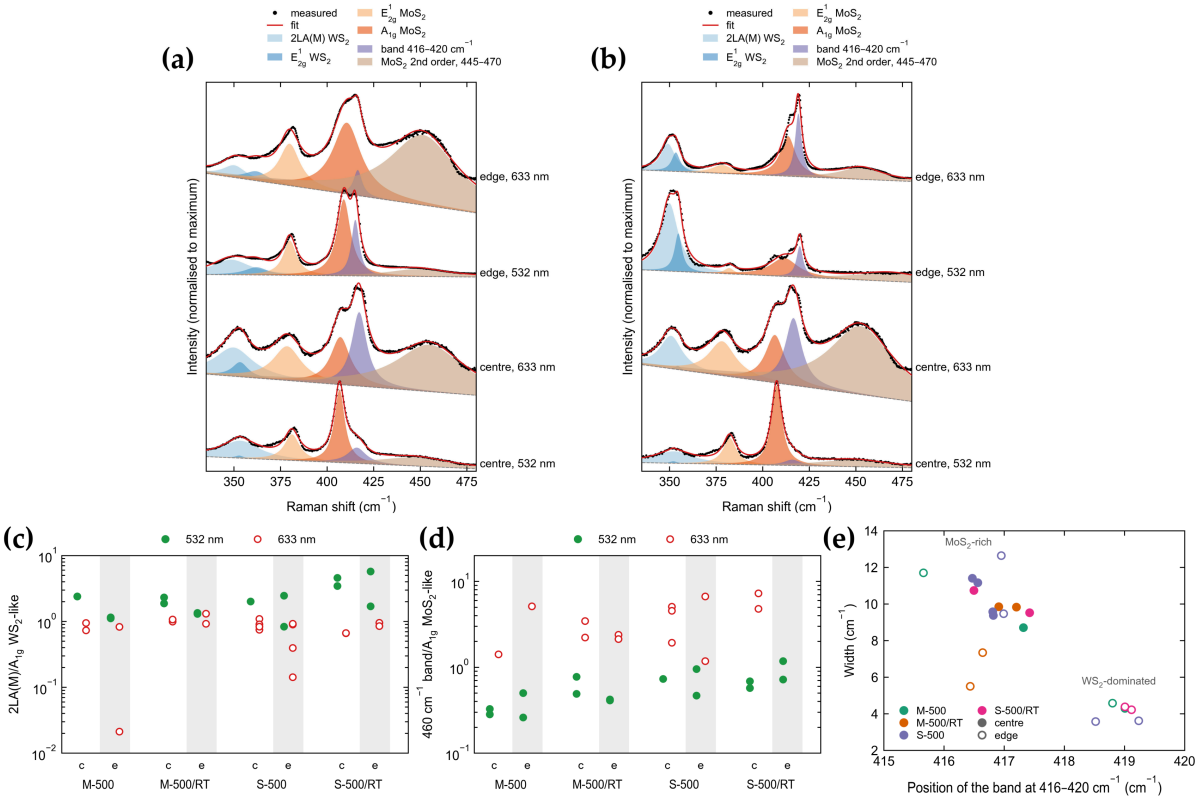


Figure 8. Raman spectra at 532 and 633 nm of the films deposited at 500 °C and sulphurised at 650 °C. (**a**) Spectra (points) of M-500/RT at the centre and near the edge at both wavelengths, each normalised to its maximum between 335 and 480 cm^{-1} and vertically offset, with the six-component Lorentzian fits (red), their components (filled, WS_2 bands in blue, MoS_2 bands in orange, the band at 416 to 420 cm^{-1} in purple and the second-order MoS_2 band at 445 to 470 cm^{-1} in brown) and the linear background (dashed). (**b**) The same for S-500/RT. (**c**) Ratio of the integrated areas of the 2LA(M) and WS_2-like A_{1g} bands for every measured spot, grouped by film, centre (c) and edge (e, shaded), at 532 nm (filled) and 633 nm (open). (**d**) Ratio of the integrated areas of the band at 445 to 470 cm^{-1} and the MoS_2-like A_{1g} band, as in (**c**), for the spots in which the MoS_2-like A_{1g} was resolved. (**e**) Width against position of the band between 416 and 420 cm^{-1} at 633 nm, for every spot, filled for centre and open for edge.

At 633 nm, the band between 416 and 420 cm^{-1} was either narrow or broad, depending on the spot (Figure 8e). In the spots dominated by WS_2—two edge spots of S-500, both edge spots of S-500/RT, and one centre and one edge spot of M-500—it was narrow (3.6 to 4.6 cm^{-1}) and was at 418.5 to 419.2 cm^{-1}, as expected for the A_{1g} band of WS_2. In the spots rich in MoS_2—all centre spots of M-500/RT, S-500 and S-500/RT, the other two edge spots of S-500 and the other two spots of M-500—it was broad (8.7 to 12.6 cm^{-1}) and was at lower wavenumbers, 415.7 to 417.4 cm^{-1}. At 1.96 eV, the second-order band c of MoS_2

near 418 cm^{-1} is among the most strongly enhanced features of MoS_2 [37], and it coincides with the WS_2-like A_{1g} band. The broad band is therefore attributed to a superposition of the two. This attribution is consistent with the centre of S-500/RT, where both spectra at 532 nm were nearly pure MoS_2 (Table 7) but both spectra at 633 nm contained the broad band with an area 1.2 to 3.3 times that of the MoS_2-like A_{1g} band.

Table 8. Raman band parameters of the films sulphurised at 650 °C at 532 and 633 nm, by zone, from six-component Lorentzian fits between 335 and 480 cm^{-1}. Ranges are over the spots of each zone. The band between 416 and 420 cm^{-1} contains the WS_2-like A_{1g} band and, at 633 nm, the second-order band c of MoS_2. Ratios are of integrated areas. "Shoulder" denotes spots in which the MoS_2-like A_{1g} band was only a shoulder of the WS_2 band and is left out of the A_{1g} and 460 cm^{-1} columns.

Film	Zone	Line (nm)	Spots	A_{1g} MoS_2-like (cm^{-1})	Band at 416–420 cm^{-1} (cm^{-1})	Width (cm^{-1})	2LA(M)/A_{1g} WS_2-like	460 cm^{-1} Band/ A_{1g} MoS_2-like
M-500	centre	532	2	407.4–408.1	417.6–418.0	6.4–6.8	2.39–2.40	0.28–0.33
		633	2	407.9 (1 shoulder)	417.3–419.0	4.3–8.7	0.73–0.95	1.41
	edge	532	2	409.1–410.1	414.5–416.3	5.1–6.1	1.11–1.15	0.26–0.50
		633	2	407.3 (1 shoulder)	415.7–418.8	4.6–11.7	0.02–0.83	5.13
M-500/RT	centre	532	2	406.6–407.3	415.9–416.8	8.7–12.0	1.88–2.31	0.49–0.78
		633	2	407.1–407.5	416.9–417.2	9.8	0.99–1.07	2.22–3.46
	edge	532	2	408.5–408.9	415.1–416.0	5.2–6.8	1.30–1.34	0.41–0.42
		633	2	409.4–410.6	416.4–416.6	5.5–7.3	0.92–1.31	2.13–2.39
S-500	centre	532	1	407.2	416.2	11.2	2.00	0.73
		633	4	404.5–406.5 (1 shoulder)	416.5–416.8	9.4–11.4	0.75–1.09	1.93–5.06
	edge	532	2	407.6–413.2	416.9–418.7	3.3–10.6	0.83–2.46	0.47–0.95
		633	4	403.5–406.3 (2 shoulder)	416.9–419.2	3.6–12.6	0.14–0.92	1.18–6.67
S-500/RT	centre	532	2	406.3–407.5	415.9–419.1	11.0–17.8	3.46–4.57	0.57–0.69
		633	2	405.7–406.5	416.5–417.4	9.5–10.7	0.66–0.67	4.79–7.27
	edge	532	2	411.1–411.5	418.5–419.9	4.3–5.1	1.70–5.72	0.72–1.18
		633	2	- (2 shoulder)	419.0–419.1	4.2–4.4	0.85–0.95	-

The band positions are less affected by these resonances. At the edge of M-500/RT, the MoS_2-like A_{1g} band was at 409.4 to 410.6 cm^{-1} at 633 nm against 407.1 to 407.5 cm^{-1} at the centre, and the separation of the two A_{1g} bands was 5.9 to 7.3 cm^{-1} against 9.4 to 10.1 cm^{-1} at the centre. These values reproduce those at 532 nm (6.2 to 7.5 against 9.3 to 9.5 cm^{-1}), so the convergence of the two A_{1g} bands at the edge of M-500/RT is observed at both lines. For M-500, the test could not be repeated at 633 nm, because one centre spot and one edge spot were dominated by WS_2, with the MoS_2-like A_{1g} band reduced to a shoulder.

In the sulphide films, the separation of the two A_{1g} bands at 633 nm was 10.0 to 13.5 cm^{-1} wherever both were resolved, so the sulphide films showed no convergence at either line. The spectra at both excitation lines thus show the A_{1g} convergence in the same zones, while the relative intensities of the MoS_2-like and WS_2-like bands depend strongly on the excitation line. This different response of MoS_2-like and WS_2-like domains to the two excitation energies reflects their different excitonic resonances, so the spot-to-spot variation in composition of the sulphide films is detected at both lines.

4. Discussion

4.1. The Processing Window

For the stacks deposited at room temperature, the Raman spectra showed separate bands of the two disulphides between 550 and 650 °C at the sample centre. In this range, sulphurisation of both precursors produced crystalline, basal-plane textured films, and the separation of the two A_{1g} bands was 9.3 to 10.3 cm^{-1}, with the MoS_2-like band at the position of bulk MoS_2 (Table 4). The WS_2-like A_{1g} band was 2.5 to 3.4 cm^{-1} below the bulk value, a shift that thinning alone produces in WS_2 [32] and that is therefore not taken as

evidence of mixing. The convergence criterion separates the two cases, because intermixing increases the wavenumber of the MoS_2-like A_{1g} band and decreases that of the WS_2-like one, whereas thinning decreases only that of the WS_2-like band [33]. By this criterion, mixing was not detected at the centre of the samples up to 650 °C.

The lower limit of the window depends on the precursor. Both disulphides formed from the metallic precursor at 500 °C, while in the sulphide precursor, the WS_x layer did not crystallise at 500 °C and oxide reflections remained (Sections 3.3 and 3.4). From 550 °C, both precursors were fully sulphurised, in agreement with thin Mo and W films sulphurised for 15 min, which reached approximately 80% stoichiometric disulphide at 550 °C [17]. A sulphurisation temperature of 550 °C is well below the 750 to 800 °C typical for the sulphurisation of thin Mo oxide films [40] and the 1000 °C used to obtain nearly oxide-free WS_2 from sputtered W in a hydrogen-containing atmosphere [41]. The sulphur supply determines whether planar MoS_2 or segregated oxide forms [13], and the confined box maintains a high local sulphur pressure with a small sulphur charge, which is the most likely reason for complete sulphurisation at 550 °C without hydrogen. The range is therefore 500 to 650 °C for the metallic stacks and 550 to 650 °C for the sulphide stacks, in both cases at the sample centre.

The upper limit corresponds to the convergence of the A_{1g} bands detected at 700 °C, so the onset is between 650 and 700 °C. At 700 °C, the MoS_2-like A_{1g} band of the metallic series shifted to higher wavenumber by 2.8 cm^{-1} and the separation of the two A_{1g} bands decreased from 9.4 to 6.2 cm^{-1}, while the sulphide series showed the same convergence to a smaller extent, from 9.8 to 8.5 cm^{-1} (Table 4). The WS_2-like band moved to lower wavenumber by 0.4 cm^{-1} in the metallic series and 0.9 cm^{-1} in the sulphide series. Increasing thickness stiffens the A_{1g} mode [31], so that the growth of the crystallites cannot account for this shift, or for the position of the MoS_2-like band of the metallic series, 3.2 cm^{-1} above the bulk value. A homogeneous strain would displace the two A_{1g} bands in the same direction, whereas they moved in opposite directions. An increased defect density is not supported by the XRD, since the area of the 002 reflection increased and the higher-order reflections appeared. Mixing is therefore the most likely explanation. The convergence coincided with a change in the film structure. The crystallite size perpendicular to the substrate doubled to 10.5 to 10.8 nm, larger than the film thickness at lower temperatures, the higher-order 00l reflections appeared, and the XRR fringes were damped so strongly that no fit was possible (Sections 3.2 and 3.3). In-plane Mo hopping in crystalline MoS_2 has a barrier of approximately 2.9 eV [42], so lattice diffusion inside a completed disulphide is too slow to mix the layers in 15 min. We propose that mixing at 700 °C takes place during the recrystallisation of the film through its whole thickness, along the boundaries of the growing crystallites. In lateral MoS_2-WS_2 heterostructures grown by chemical vapour deposition, the $Mo_{1-x}W_xS_2$ alloy at the junction extends over tens of nanometres and contains vacancies, crystal edges and distinct nanocrystallites [43]. Both precursors were amorphous and of low density (Table 2). Between 550 and 650 °C, D_0 changed from 4.3 to 5.1 nm in the metallic series and from 4.7 to 5.7 nm in the sulphide series, at constant total thickness. D_0 was close to the thickness of one layer in the sulphide series, and 70 to 89% of the total thickness in the metallic series, so that coherent stacking extends across the former interface in the metallic films. At 700 °C, D_0 exceeded the thickness measured at lower temperatures and the XRR fringes were damped, which indicates a reconstruction of the entire film.

The window was determined at the centre of the samples. For the room-temperature series, no spectra were recorded near the edges, so it is not known whether the room-temperature films also mixed at the edges below 700 °C. In the metallic stacks deposited at 500 °C, the A_{1g} bands converged near the edges after sulphurisation at 650 °C, to a separation of 5.4 to 7.4 cm^{-1}, against 9.0 to 10.2 cm^{-1} at the centre (Table 7), and the convergence

was the same at 633 nm for M-500/RT (Section 3.6). For the metallic stacks deposited at 500 °C, the upper limit of the window is therefore lower at the edges than at the centre. The sulphide stacks deposited at 500 °C, sulphurised in the same box on substrates of the same size, showed no convergence near the edges. A temperature difference at the edge acting alone would be expected to affect both chemistries, so the effect depends on the metallic precursor and is compatible with a different local sulphur supply near the edges. A thinner deposit near the edges is the second possible cause.

4.2. Comparison with Earlier Reports on Sulphurised Mo/W Stacks

The onset at 700 °C agrees with the uniform $Mo_{0.5}W_{0.5}S_2$ film obtained from a Mo (1.2 nm)/W (1.2 nm) stack sulphurised at the same temperature [21], where the metal layers had nearly the same nominal thickness as our metallic precursor (1.07 nm each). Sequentially sputtered Mo and W films also resulted in $Mo_{1-x}W_xS_2$ alloys during chemical vapour deposition, with a composition determined by the thickness ratio and the stacking order of the two metals [44]. The onset at 700 °C is below the 800 to 850 °C at which our earlier MoS_x/W stacks formed vertically graded $Mo_{1-x}W_xS_2$ [22], which is consistent with mixing that increases with temperature once it has started. Vertically graded $Mo_{1-x}W_xS_2$ films can also be deposited directly, by gradient aerosol-assisted chemical vapour deposition [45].

Several studies reported no mixing at comparable or higher temperatures. A W and Mo stack sulphurised at 750 °C for 15 min showed separate MoS_2 and WS_2 Raman modes [20], and WO_{3-x}/MoO_{3-x} bilayers grown by pulsed laser deposition and sulphurised at 900 °C resulted in WS_2/MoS_2 heterostructures whose Raman band positions matched those of the separate layers [46]. Separate modes do not exclude partial mixing, since sulphurised few-layer $Mo_{1-x}W_xS_2$ films show two-mode behaviour of both E^1_{2g} and A_{1g} [47], so the separation of the two A_{1g} bands is the measure of mixing. In our films, the two bands also remained resolved at 700 °C, and only their convergence indicated the mixing. Mo sputtered on W and sulphurised at 600 °C for 2 h showed atomically sharp MoS_2/WS_2 interfaces in cross-sectional HRTEM and separated Mo and W in STEM-EDS [19]. This result is consistent with our window, which extends to 650 °C. The processes also differ. The stack was sulphurised in flowing Ar at low pressure, while our samples were sulphurised in a confined box, and our Mo films were oxidised before sulphurisation (Section 4.3). In our earlier MoS_x/W films sulphurised at 800 to 850 °C, whose A_{1g} bands formed one broad band, cross-sectional STEM-EDX found both metals through the film thickness and resolved a vertical composition gradient, at an effective resolution of a few nanometres [22]. Angle-resolved XPS of the same films probed only the topmost few nanometres [22]. Both resolutions are comparable to the 3 to 5 nm thickness of the individual layers in the present stacks. The A_{1g} band positions, which respond to the mixing of Mo and W on the metal sublattice, are therefore used here as the criterion for mixing.

4.3. Effect of Depositing the Precursors at 500 °C

Precursors deposited at 500 °C, with nominal layer thicknesses of 2.14 nm (metallic) and 9.6 nm (sulphide) against 1.07 and 4.8 nm for the room-temperature precursors, were sulphurised at 650 °C. They showed no larger separation of the A_{1g} bands than the room-temperature films. Deposition at 500 °C changed the precursors in three ways.

First, the Mo layer of M-500/RT, deposited at room temperature on W deposited at 500 °C, was fully oxidised before sulphurisation. The best XRR model of the M-500/RT precursor contained 7.1 nm of oxide at 4.5 g/cm^3, close to the 7.0 nm of MoO_3 expected from the nominal 2.14 nm of Mo, while the Mo deposited at 500 °C in M-500 retained a 1.53 nm layer at 9.5 g/cm^3 under 1.96 nm of oxide (Section 3.5.1). The Mo-based layer of the room-temperature precursor M-RT had a density of 6.4 g/cm^3, 63% of bulk Mo (Table 2). Films

sputtered at a low ratio of substrate to melting temperature grow as columns separated by voids [48], and in such a porous structure the whole layer is in contact with air, while the denser Mo deposited at 500 °C oxidised only at its surface. After sulphurisation, M-500/RT reached the thickness expected from full sulphurisation of its metal content, while M-500 reached 59 ± 2% of this thickness (Table 5). The 002 reflection of M-500/RT was nevertheless eight times weaker than that of M-500, with a similar crystallite size, so that a smaller fraction of the thicker M-500/RT film was crystalline and textured. The low mean density of its WS_2 layer in the XRR fit, 5.2 against 7.5 g/cm^3 for bulk WS_2, is consistent with this.

Second, half of the MoS_x deposited at 500 °C did not remain on the substrate. After sulphurisation, S-500 was 5.1 ± 0.5 nm thinner than S-500/RT, whose WS_x layer had been deposited under the same conditions and whose MoS_2 layer was 9.8 nm thick (Section 3.5). Sulphur desorbs from MoS_2 sputtered at substrate temperatures above 300 °C [49], and partially reduced Mo oxide becomes volatile in sulphur vapour near 500 °C, whereas W oxide does not [50]. Either mechanism can account for the smaller amount of Mo after deposition at 500 °C.

Third, deposition at 500 °C did not prevent convergence of the A_{1g} bands. The metallic stacks deposited at 500 °C showed this convergence near the edges at 650 °C (Section 4.1), whereas the sulphide stacks deposited at 500 °C showed no A_{1g} convergence at either excitation line. Grain-boundary diffusion of Mo in W is three to seven orders of magnitude faster than volume diffusion [51], and a few-nanometre film deposited at 500 °C is still nanocrystalline, so a hot deposition does not remove the fast paths for Mo-W interdiffusion.

4.4. Comparison of the 532 and 633 nm Excitation

The comparison of the 532 and 633 nm excitation (Section 3.6) supports the use of band positions, and not band intensities, as the measure of Mo-W mixing in the sulphurised MoS_2/WS_2 films. The ratio of the 2LA(M) to A_{1g} intensities of WS_2 decreased from a median of 2.0 at 532 nm to 0.9 at 633 nm, which shows that the strong 2LA(M) band at 532 nm reflects the resonance of thin WS_2 domains near 2.4 eV [32] and not alloying. At 633 nm, the intensity near 418 cm^{-1} includes a resonant second-order band of MoS_2 [37], so that intensity ratios at this wavelength are not used to determine the composition. The positions of the two A_{1g} bands, in contrast, showed the same convergence at the edge of M-500/RT at both wavelengths. The different resonance response of MoS_2-like and WS_2-like domains is itself a consequence of their different excitonic transitions, which is why the two lines distinguish them even where intensities cannot be translated into composition.

For heterostructure devices, the window defines the conditions in which the two disulphides remain separate, and with them the type II band offset between MoS_2 and WS_2 on which charge separation depends [4,5]. Above the window, the composition, and therefore the band gap, vary across the former interface [9,10]. Sulphurisation at 550 to 650 °C results in separate MoS_2 and WS_2 Raman bands, and sulphurisation at 700 °C results in a mixed or graded film.

5. Conclusions

Metallic Mo/W and sulphide MoS_x/WS_x stacks deposited by magnetron sputtering were sulphurised in a confined graphite box for 15 min at temperatures ranging from 500 to 700 °C. For precursors deposited at room temperature, sulphurisation between 550 and 650 °C produced crystalline, textured MoS_2 and WS_2 from both layers, and the separation of the two A_{1g} Raman bands was 9.3 to 10.3 cm^{-1} at the sample centre. The lower limit depends on the precursor. Both disulphides already formed from the metallic stack at 500 °C, while the WS_x layer of the sulphide stack did not crystallise at this temperature. The

upper limit corresponds to the convergence of the A_{1g} bands at 700 °C, which we attribute to Mo-W mixing with an onset between 650 and 700 °C, and which coincided with a doubling of the crystallite size and XRR curves that could no longer be fitted with a layer model.

Precursors with one or both layers deposited at 500 °C and sulphurised at 650 °C showed no larger separation of the A_{1g} bands. The XRR is consistent with full oxidation of the Mo layer deposited at room temperature on W deposited at 500 °C, half of the MoS_x deposited at 500 °C remained on the substrate, and the metallic stacks deposited at 500 °C showed convergence of the A_{1g} bands near the sample edges at 650 °C. The Raman spectra at 532 and 633 nm showed that the strong WS_2 2LA(M) band is a resonance effect and that intensity ratios at 633 nm are affected by a second-order MoS_2 band, while the positions of the two A_{1g} bands identify mixing consistently at both wavelengths.

The MoS_2/WS_2 heterostructures with separate MoS_2 and WS_2 Raman bands can therefore be obtained from sputtered precursors in a single sulphurisation step at 550 to 650 °C, provided the precursors are deposited at room temperature. The window is defined here by Raman spectroscopy. Composition profiles measured on cross-sections and Raman maps would allow the limits of the window and the vertical distribution of Mo and W to be determined directly.

Author Contributions: Conceptualization, A.V., F.S. and C.M.; methodology, F.S., I.-D.S. and A.V.; software, A.V.; formal analysis, A.V. and F.S.; investigation, I.-D.S., F.S. and M.Y.Z.; resources, A.V., C.M. and D.N.B.B.; data curation, F.S. and A.V.; writing—original draft preparation, A.V.; writing—review and editing, A.V., F.S., I.-D.S., C.M., M.Y.Z. and D.N.B.B.; visualisation, A.V.; supervision, A.V.; project administration, A.V. and C.M.; funding acquisition, A.V., C.M. and D.N.B.B. All authors have read and agreed to the published version of the manuscript.

Funding: This research was funded by the Core Program of the National Institute of Materials Physics, granted by the Romanian Ministry of Research, Innovation and Digitization through Project PC3-PN23080303, and by the Executive Unit for Financing Higher Education, Research, Development and Innovation (UEFISCDI) within the framework of Project PN-IV-P7-7.1-PED-2024-2412 (Contract No. 11PED/2025).

Data Availability Statement: The original contributions presented in this study are included in the article. Further inquiries can be directed to the corresponding author.

Acknowledgments: During the preparation of this manuscript, the authors used Claude Opus 5.5 (Anthropic), for the purposes of searching the published literature, compiling candidate references, and checking the text for consistency and language. The authors have reviewed and edited the output and take full responsibility for the content of this publication. Every reference was checked against the original source. All claims, interpretations and conclusions are those of the authors.

Conflicts of Interest: Author Dan Nicolae Becherescu Barbu was employed by the company Phanos Technology S.R.L. The remaining authors declare that the research was conducted in the absence of any commercial or financial relationships that could be construed as a potential conflict of interest.

References

1. Wang, Q.H.; Kalantar-Zadeh, K.; Kis, A.; Coleman, J.N.; Strano, M.S. Electronics and optoelectronics of two-dimensional transition metal dichalcogenides. *Nat. Nanotechnol.* **2012**, *7*, 699–712. [CrossRef] [PubMed]
2. Geim, A.K.; Grigorieva, I.V. Van der Waals heterostructures. *Nature* **2013**, *499*, 419–425. [CrossRef] [PubMed]
3. Novoselov, K.S.; Mishchenko, A.; Carvalho, A.; Castro Neto, A.H. 2D materials and van der Waals heterostructures. *Science* **2016**, *353*, aac9439. [CrossRef] [PubMed]
4. Kang, J.; Tongay, S.; Zhou, J.; Li, J.; Wu, J. Band offsets and heterostructures of two-dimensional semiconductors. *Appl. Phys. Lett.* **2013**, *102*, 012111. [CrossRef]
5. Hong, X.; Kim, J.; Shi, S.-F.; Zhang, Y.; Jin, C.; Sun, Y.; Tongay, S.; Wu, J.; Zhang, Y.; Wang, F. Ultrafast charge transfer in atomically thin MoS_2/WS_2 heterostructures. *Nat. Nanotechnol.* **2014**, *9*, 682–686. [CrossRef] [PubMed]

6. Chen, H.; Wen, X.; Zhang, J.; Wu, T.; Gong, Y.; Zhang, X.; Yuan, J.; Yi, C.; Lou, J.; Ajayan, P.M.; et al. Ultrafast formation of interlayer hot excitons in atomically thin MoS_2/WS_2 heterostructures. *Nat. Commun.* **2016**, *7*, 12512. [CrossRef] [PubMed]
7. Dumcenco, D.O.; Kobayashi, H.; Liu, Z.; Huang, Y.-S.; Suenaga, K. Visualization and quantification of transition metal atomic mixing in $Mo_{1-x}W_xS_2$ single layers. *Nat. Commun.* **2013**, *4*, 1351. [CrossRef] [PubMed]
8. Gan, L.-Y.; Zhang, Q.; Zhao, Y.-J.; Cheng, Y.; Schwingenschlögl, U. Order-disorder phase transitions in the two-dimensional semiconducting transition metal dichalcogenide alloys $Mo_{1-x}W_xX_2$ (X = S, Se and Te). *Sci. Rep.* **2014**, *4*, 6691. [CrossRef] [PubMed]
9. Chen, Y.; Xi, J.; Dumcenco, D.O.; Liu, Z.; Suenaga, K.; Wang, D.; Shuai, Z.; Huang, Y.-S.; Xie, L. Tunable band gap photoluminescence from atomically thin transition-metal dichalcogenide alloys. *ACS Nano* **2013**, *7*, 4610–4616. [CrossRef] [PubMed]
10. Song, J.-G.; Ryu, G.H.; Lee, S.J.; Sim, S.; Lee, C.W.; Choi, T.; Jung, H.; Kim, Y.; Lee, Z.; Myoung, J.-M.; et al. Controllable synthesis of molybdenum tungsten disulfide alloy for vertically composition-controlled multilayer. *Nat. Commun.* **2015**, *6*, 7817. [CrossRef] [PubMed]
11. Kang, K.; Xie, S.; Huang, L.; Han, Y.; Huang, P.Y.; Mak, K.F.; Kim, C.-J.; Muller, D.; Park, J. High-mobility three-atom-thick semiconducting films with wafer-scale homogeneity. *Nature* **2015**, *520*, 656–660. [CrossRef] [PubMed]
12. Orofeo, C.M.; Suzuki, S.; Sekine, Y.; Hibino, H. Scalable synthesis of layer-controlled WS_2 and MoS_2 sheets by sulfurization of thin metal films. *Appl. Phys. Lett.* **2014**, *105*, 083112. [CrossRef]
13. Wu, C.-R.; Chang, X.-R.; Wu, C.-H.; Lin, S.-Y. The growth mechanism of transition metal dichalcogenides by using sulfurization of pre-deposited transition metals and the 2D crystal hetero-structure establishment. *Sci. Rep.* **2017**, *7*, 42146. [CrossRef] [PubMed]
14. Hussain, S.; Singh, J.; Vikraman, D.; Singh, A.K.; Iqbal, M.Z.; Khan, M.F.; Kumar, P.; Choi, D.-C.; Song, W.; An, K.-S.; et al. Large-area, continuous and high electrical performances of bilayer to few layers MoS_2 fabricated by RF sputtering via post-deposition annealing method. *Sci. Rep.* **2016**, *6*, 30791. [CrossRef] [PubMed]
15. Ishihara, S.; Hibino, Y.; Sawamoto, N.; Suda, K.; Ohashi, T.; Matsuura, K.; Machida, H.; Ishikawa, M.; Sudoh, H.; Wakabayashi, H.; et al. Properties of single-layer MoS_2 film fabricated by combination of sputtering deposition and post deposition sulfurization annealing using $(t\text{-}C_4H_9)_2S_2$. *Jpn. J. Appl. Phys.* **2016**, *55*, 06GF01. [CrossRef]
16. Mihai, C.; Simandan, I.-D.; Sava, F.; Tite, T.; Bocirnea, A.; Vaduva, M.; Zaki, M.Y.; Baibarac, M.; Velea, A. Fabrication of high-quality MoS_2/graphene lateral heterostructure memristors. *Nanomaterials* **2025**, *15*, 1239. [CrossRef] [PubMed]
17. Gu, Y.; Serna, M.I.; Mohan, S.; Londoño-Calderon, A.; Ahmed, T.; Huang, Y.; Lee, J.; Walia, S.; Pettes, M.T.; Liechti, K.M.; et al. Sulfurization engineering of one-step low-temperature MoS_2 and WS_2 thin films for memristor device applications. *Adv. Electron. Mater.* **2022**, *8*, 2100515. [CrossRef]
18. Zhu, J.; Park, J.-H.; Vitale, S.A.; Ge, W.; Jung, G.S.; Wang, J.; Mohamed, M.; Zhang, T.; Ashok, M.; Xue, M.; et al. Low-thermal-budget synthesis of monolayer molybdenum disulfide for silicon back-end-of-line integration on a 200 mm platform. *Nat. Nanotechnol.* **2023**, *18*, 456–463. [CrossRef] [PubMed]
19. Choudhary, N.; Park, J.; Hwang, J.Y.; Chung, H.-S.; Dumas, K.H.; Khondaker, S.I.; Choi, W.; Jung, Y. Centimeter scale patterned growth of vertically stacked few layer only 2D MoS_2/WS_2 van der Waals heterostructure. *Sci. Rep.* **2016**, *6*, 25456. [CrossRef] [PubMed]
20. Woods, J.M.; Jung, Y.; Xie, Y.; Liu, W.; Liu, Y.; Wang, H.; Cha, J.J. One-step synthesis of MoS_2/WS_2 layered heterostructures and catalytic activity of defective transition metal dichalcogenide films. *ACS Nano* **2016**, *10*, 2004–2009. [CrossRef] [PubMed]
21. Panasci, S.E.; Schilirò, E.; Koos, A.; Kutlu, T.; Sahin, H.; Roccaforte, F.; Pécz, B.; Giannazzo, F. Scalable growth of optically uniform $MoWS_2$ alloys by sulfurization of ultrathin Mo/W stacks. *Mater. Sci. Semicond. Process.* **2025**, *196*, 109648. [CrossRef]
22. Velea, A.; Simandan, I.-D.; Mihai, C.; Baibarac, M.; Vaduva, M.; Negrila, C.C.; Tite, T.; Kuncser, A.; Sava, F. Direct synthesis of vertically graded $Mo_{1-x}W_xS_2$ multilayer alloys by confined-space sulphurisation of magnetron-sputtered MoS_x/W precursors. *Nanoscale* **2026**, *18*, 19143–19156. [CrossRef] [PubMed]
23. Xue, Y.; Zhang, Y.; Liu, Y.; Liu, H.; Song, J.; Sophia, J.; Liu, J.; Xu, Z.; Xu, Q.; Wang, Z.; et al. Scalable production of a few-layer MoS_2/WS_2 vertical heterojunction array and its application for photodetectors. *ACS Nano* **2016**, *10*, 573–580. [CrossRef] [PubMed]
24. Al Qaydi, M.; Kotbi, A.; Rajput, N.S.; Bouchalkha, A.; El Marssi, M.; Matras, G.; Kasmi, C.; Jouiad, M. Photodetection properties of MoS_2, WS_2 and $Mo_xW_{1-x}S_2$ heterostructure: A comparative study. *Nanomaterials* **2023**, *13*, 24. [CrossRef] [PubMed]
25. Mihai, C.; Simandan, I.-D.; Sava, F.; Buruiana, A.-T.; Bocirnea, A.E.; Tite, T.; Zaki, M.Y.; Velea, A. Synthesis of wrinkled MoS_2 thin films using a two-step method consisting of magnetron sputtering and sulfurization in a confined space. *Sustainability* **2024**, *16*, 3819. [CrossRef]
26. Sava, F.; Simandan, I.-D.; Buruiana, A.-T.; Bocirnea, A.E.; El Khouja, O.; Tite, T.; Zaki, M.Y.; Mihai, C.; Velea, A. Synthesis of WS_2 ultrathin films by magnetron sputtering followed by sulfurization in a confined space. *Surfaces* **2024**, *7*, 108–119. [CrossRef]
27. Velea, A.; Simandan, I.-D.; Mihai, C.; Baibarac, M.; Vaduva, M.; Udrescu, A.; Smaranda, I.; Bocirnea, A.E.; Tite, T.; Zaki, M.Y.; et al. Large-scale synthesis of monolayer WS_2 by low-temperature sulfurization of oxidized magnetron sputtered monolayer W precursors in a microreactor. *Nanotechnology* **2025**, *36*, 265601. [CrossRef] [PubMed]
28. Parratt, L.G. Surface studies of solids by total reflection of X-rays. *Phys. Rev.* **1954**, *95*, 359–369. [CrossRef]

29. Névot, L.; Croce, P. Caractérisation des surfaces par réflexion rasante de rayons X. Application à l'étude du polissage de quelques verres silicates. *Rev. Phys. Appl.* **1980**, *15*, 761–779. [CrossRef]
30. Chantler, C.T. Theoretical form factor, attenuation, and scattering tabulation for Z = 1-92 from E = 1–10 eV to E = 0.4–1.0 MeV. *J. Phys. Chem. Ref. Data* **1995**, *24*, 71–643. [CrossRef]
31. Lee, C.; Yan, H.; Brus, L.E.; Heinz, T.F.; Hone, J.; Ryu, S. Anomalous lattice vibrations of single- and few-layer MoS_2. *ACS Nano* **2010**, *4*, 2695–2700. [CrossRef] [PubMed]
32. Berkdemir, A.; Gutiérrez, H.R.; Botello-Méndez, A.R.; Perea-López, N.; Elías, A.L.; Chia, C.-I.; Wang, B.; Crespi, V.H.; López-Urías, F.; Charlier, J.-C.; et al. Identification of individual and few layers of WS_2 using Raman spectroscopy. *Sci. Rep.* **2013**, *3*, 1755. [CrossRef]
33. Schulpen, J.J.P.M.; Verheijen, M.A.; Kessels, W.M.M.; Vandalon, V.; Bol, A.A. Controlling transition metal atomic ordering in two-dimensional $Mo_{1-x}W_xS_2$ alloys. *2D Mater.* **2022**, *9*, 025016. [CrossRef]
34. Chen, Y.; Dumcenco, D.O.; Zhu, Y.; Zhang, X.; Mao, N.; Feng, Q.; Zhang, M.; Zhang, J.; Tan, P.-H.; Huang, Y.-S.; et al. Composition-dependent Raman modes of $Mo_{1-x}W_xS_2$ monolayer alloys. *Nanoscale* **2014**, *6*, 2833–2839. [CrossRef] [PubMed]
35. Zhao, W.; Ghorannevis, Z.; Amara, K.K.; Pang, J.R.; Toh, M.; Zhang, X.; Kloc, C.; Tan, P.H.; Eda, G. Lattice dynamics in mono- and few-layer sheets of WS_2 and WSe_2. *Nanoscale* **2013**, *5*, 9677–9683. [CrossRef] [PubMed]
36. Staiger, M.; Gillen, R.; Scheuschner, N.; Ochedowski, O.; Kampmann, F.; Schleberger, M.; Thomsen, C.; Maultzsch, J. Splitting of monolayer out-of-plane A1′ Raman mode in few-layer WS_2. *Phys. Rev. B* **2015**, *91*, 195419. [CrossRef]
37. Lee, J.-U.; Park, J.; Son, Y.-W.; Cheong, H. Anomalous excitonic resonance Raman effects in few-layered MoS_2. *Nanoscale* **2015**, *7*, 3229–3236. [CrossRef] [PubMed]
38. Carvalho, B.R.; Malard, L.M.; Alves, J.M.; Fantini, C.; Pimenta, M.A. Symmetry-dependent exciton-phonon coupling in 2D and bulk MoS_2 observed by resonance Raman scattering. *Phys. Rev. Lett.* **2015**, *114*, 136403. [CrossRef] [PubMed]
39. Livneh, T.; Spanier, J.E. A comprehensive multiphonon spectral analysis in MoS_2. *2D Mater.* **2015**, *2*, 035003. [CrossRef]
40. Panasci, S.E.; Koos, A.; Schilirò, E.; Di Franco, S.; Greco, G.; Fiorenza, P.; Roccaforte, F.; Agnello, S.; Cannas, M.; Gelardi, F.M.; et al. Multiscale investigation of the structural, electrical and photoluminescence properties of MoS_2 obtained by MoO_3 sulfurization. *Nanomaterials* **2022**, *12*, 182. [CrossRef] [PubMed]
41. Fedorenko, A.D.; Lavrukhina, S.A.; Alekseev, V.A.; Sysoev, V.I.; Sulyaeva, V.S.; Okotrub, A.V.; Bulusheva, L.G. Thin films of tungsten disulfide grown by sulfurization of sputtered metal for ultra-low detection of nitrogen dioxide gas. *Nanomaterials* **2025**, *15*, 594. [CrossRef] [PubMed]
42. Hong, J.; Pan, Y.; Hu, Z.; Lv, D.; Jin, C.; Ji, W.; Yuan, J.; Zhang, Z. Direct imaging of kinetic pathways of atomic diffusion in monolayer molybdenum disulfide. *Nano Lett.* **2017**, *17*, 3383–3390. [CrossRef] [PubMed]
43. Kim, D.H.; Lee, C.; Kim, S.H.; Jeong, B.G.; Yun, S.J.; Suh, H.C.; Lee, D.; Kim, K.K.; Jeong, M.S. Probing the multi-disordered nanoscale alloy at the interface of lateral heterostructure of MoS_2-WS_2. *Nanophotonics* **2024**, *13*, 1069–1077. [CrossRef] [PubMed]
44. Poston, W.; Bizhani, M.; Jensen, G.; Aldosari, N.; Tariq, M.; Kordesch, M.; Aleithan, S.; Stinaff, E. Thin-film transition metal dichalcogenide alloys grown by patterned films of stacked Mo and W. *Mater. Lett.* **2025**, *386*, 138231. [CrossRef]
45. Barde, A.; Al-Jurani, H.S.; Ward-O'Brien, B.; Buckingham, M.A.; Cernik, R.; Lewis, D.J. Gradient aerosol chemical vapor deposition (GA-CVD) for vertically graded thin films of $Mo_xW_{1-x}S_2$ and $W_xMo_{1-x}S_2$. *Chem. Commun.* **2025**, *61*, 4407–4410. [CrossRef] [PubMed]
46. Miakota, D.I.; Ghimire, G.; Canulescu, S. Laser-assisted synthesis of vertical WS_2/MoS_2 heterostructures via oxide-to-sulfide conversion. *Appl. Surf. Sci.* **2026**, *728*, 165985. [CrossRef]
47. Liu, H.; Antwi, K.K.A.; Chua, S.; Chi, D. Vapor-phase growth and characterization of $Mo_{1-x}W_xS_2$ ($0 \leq x \leq 1$) atomic layers on 2-inch sapphire substrates. *Nanoscale* **2014**, *6*, 624–629. [CrossRef] [PubMed]
48. Thornton, J.A. Influence of apparatus geometry and deposition conditions on the structure and topography of thick sputtered coatings. *J. Vac. Sci. Technol.* **1974**, *11*, 666–670. [CrossRef]
49. Imai, S.; Hamada, T.; Hamada, M.; Shirokura, T.; Muneta, I.; Kakushima, K.; Tatsumi, T.; Tomiya, S.; Tsutsui, K.; Wakabayashi, H. Importance of crystallinity improvement in MoS_2 film by compound sputtering even followed by post sulfurization. *Jpn. J. Appl. Phys.* **2021**, *60*, SBBH10. [CrossRef]
50. Wang, Z.; Liu, P.; Ito, Y.; Ning, S.; Tan, Y.; Fujita, T.; Hirata, A.; Chen, M. Chemical vapor deposition of monolayer $Mo_{1-x}W_xS_2$ crystals with tunable band gaps. *Sci. Rep.* **2016**, *6*, 21536. [CrossRef] [PubMed]
51. Hao, Y.; Tan, C.; Yu, X.; Chen, R.; Nie, Z.; Ren, Y.; Yang, S.; Li, Y.; Wang, F. Effect of grain boundary misorientation angle on diffusion behavior in molybdenum-tungsten systems. *J. Alloys Compd.* **2020**, *819*, 152975. [CrossRef]

Disclaimer/Publisher's Note: The statements, opinions and data contained in all publications are solely those of the individual author(s) and contributor(s) and not of MDPI and/or the editor(s). MDPI and/or the editor(s) disclaim responsibility for any injury to people or property resulting from any ideas, methods, instructions or products referred to in the content.